

The Inverse Kinematics of Lobster Arms

Federico Thomas*, Josep M. Porta

*Institut de Robòtica i Informàtica Industrial (CSIC-UPC)
ETSEIB, Diagonal 647, Pavelló E, planta 1, 08028 Barcelona, Spain*

Abstract

The roots of the closure polynomial associated with a given mechanism determine its assembly modes. In the case of 6R closed-loop mechanisms, these polynomials are usually expressed in the half-angle tangent of one of its joints. In this paper, we derive closure polynomials of 6R robots in terms of distances, not angles. The use of a distance-based formulation provides a fundamental advantage since it leads to closure conditions without requiring neither variable eliminations nor variable substitutions. We restrict our attention, though, to robots with coplanar consecutive joint axes, *i.e.*, robots whose consecutive axes intersect at either proper or improper points. We show that this particular arrangement of joints does not result on a reduction in the maximum number of the inverse kinematic solutions with respect to the general case. Moreover, this family of robots include broadly used offset-wrist arms. For instance, in this paper, we obtain closure polynomials for robots such as the FANUC CRX-10iA/L, the UR10e, and the KUKA LBR iiwa R800 robot in generic form (*i.e.*, as a function of their end-effector locations).

Keywords: Lobster arm, inverse kinematics, offset-wrist robots, closure polynomials, distance geometry.

1. Introduction

In 1841, in a communication addressed to the Philosophical Society of Cambridge, Robert Willis (1800-1875) showed that the joints of a common crab's claw work in the same way as those of what we would today classify as a 5R kinematic chain [1]. Willis' description appeared later summarized at the end of his influential book "*Principles of Mechanism*" [2, pp. 461-463]. This description was accompanied by the drawing in Fig. 1. He observed that the crab's claw is composed of six rigid bodies (denoted by \mathcal{A} , \mathcal{B} , \mathcal{C} , \mathcal{D} , \mathcal{E} , and \mathcal{F} in the drawing) connected in series through five revolute joints (denoted by 1, 2, 3, 4 and 5 in the drawing). What makes the arrangement of these five joint axes remarkable is that any two consecutive rotation axes in the chain intersect.

In 1979, J. Duffy and S. Derby, as a result of a suggestion by K. H. Hunt—who was aware of Willis' observations—studied the inverse kinematics of what they called the *generalized lobster arm*, a 6R kinematic chain where every two consecutive axes intersect [3] (Fig. 2(a)).

*Corresponding author at: Tel: +34 934015757. Fax: +34 934015750.

Email addresses: fthomas@iri.upc.edu (Federico Thomas), porta@iri.upc.edu (Josep M. Porta)

The resolution of this problem was seen as an intermediate step to be solved before attempting to solve the same problem for the general 6R arm which, few years earlier, was named as the “*Mount Everest of kinematic problems*” by F. Freudenstein [4]. Although rather counter-intuitive, as we will see later, the arrangement of joints in the generalized lobster arm does not provide much simplifications with respect to the general 6R arm, at least in the number of its inverse kinematic solutions. J. Duffy and S. Derby showed, using a long and complicated process, how to reduce this inverse kinematic problem to the computation of the roots of a 24th-degree polynomial. One year after, Duffy and Crane [5], based on the extended spherical geometry to dual angles, derived an input-output equation of degree 32, in one joint half-angle tangent, for the configuration of the general 7R close-loop mechanism. In other words, if one of the seven angles were regarded as the input angle, it could be said that there were at most 32 compatible values for any other angle in the kinematic loop. At that point of the story, it seemed that making consecutive axes to intersect could introduce a reduction in the number of possible solutions. Nothing was further from truth.

In 1992, V. Murthy and K. J. Waldron revisited the problem in [6]. They solved it including an important generalization: the intersection between the second and the third axis and between the fourth and the fifth axis were no longer required. They reduced the resulting system of equations to a single univariate polynomial equation of degree 16 in a way that no extraneous roots were introduced in the used variable eliminations. This implied that the end-effector could reach a given position and orientation in at most sixteen different ways. This was an important improvement with respect to Duffy and Derby’s 24th-degree polynomial solution.

Six years earlier than Murthy and Waldron’s result, E. J. F. Primrose had already proved that the general 6R robot could have up to 16 inverse kinematic solutions. However, due to the complexity of his formulation, he could not come up with a way to remove the 16 redundant solutions of a polynomial equation of degree 32 [7]. This was considered as an important landmark in the history of kinematics. Nevertheless, two years earlier, H.-Y. Lee already devised a method to explicitly obtain the 16th-degree polynomial in his Master Thesis written in Chinese [8]. This method became known to the western world when it appeared four years later in [9, 10]. Subsequently, Raghavan and Roth [11, 12] reformulated it in a cleared way using Denavit–Hartenberg (DH) parameters. Their work, based on the solution via dialytic elimination of joints variables, inspired many other polynomial approaches, such as the Gröbner basis work proposed by Wang *et al.* [13], or the eigenvalue approaches of Ghazvini [14] and Fu *et al.* [15]. Many other methods and variations have appeared since then, thus leading to an extensive literature on the topic (see, for example, [16, 17, 18, 19, 20] and the references therein). Of course, the literature also offers plenty of local numerical approaches which are not discussed here because they only allow the discovery of one solution to the problem (in general, the closest one to an initial guess). It is finally worth stressing the fact that all existing non-numerical methods reduce the problem to a univariate polynomial in the one of the joints half-angle tangent, and all the remaining joint variables follow from linear equations once the roots of the univariate polynomials are found. In this paper, we also obtain a polynomial, but in terms of a distance instead of an angle.

Certain combinations of values for the kinematic parameters of a 6R manipulator reduce the degree of its closure polynomial, and hence the number of its inverse kinematic solutions. In general, these combinations have a direct geometric interpretation in terms of orthogonality, intersection, or parallelism, of some revolute joint axes. A celebrated case is the one in which three consecutive joint axes intersect in a common point [21], or are parallel [5]. In both cases, the degree of the closure polynomial drops to eight. A detailed investigation of particular cases in which this number drops can be found in [22], where the arrangement of joint axes considered

in this paper is not included. Thus, to the best of our knowledge, the question concerning the degree of the closure polynomial of a lobster arm remains open.

Since the roots of a 16th-degree polynomial equation gives the solution of the general case, one might think that it also contains the solutions to 6R serial chains with special geometric parameters as a mere particular case. Nevertheless, as it was pointed out in [23], under certain geometric circumstances, various problems appear. Some are of numerical nature, but others are fundamental problems of the used method. Recently, it has been shown how the Raghavan and Roth method fails for 6R wrist-partitioned robots [24]. The relevance of studying particular cases has also been recently emphasized in [25] where it is argued that, while the general methods can solve all the inverse kinematics problems of 6R manipulators, at least in theory, they can hardly be implemented in industrial applications due to their high complexity [26]. In practice, 6R manipulators are usually designed with simple geometric structures. They usually have pairs of adjacent axes intersecting at a point, or perpendicular, or parallel to each other. Despite their simple structure, a universal and efficient solution to their inverse kinematic problem is needed. For that reason it is still useful to study 6R chains with special geometric parameters, such as the one discussed here.

This paper is structured as follows. In the next section, we formulate the problem in terms of distances. This will allow us to establish a kinematic connection with the 3-4 Gough-Stewart platform from which we can readily conclude that our problem can indeed have up to 16 real solutions. In Section 3, the basic operations with distances needed in the rest of the paper are summarized. These operations are used in Section 4 to derive, in few lines, a scalar algebraic radical closure condition for an arbitrary lobster arm. Then, in Section 5, it is explained how this closure condition can be expressed in polynomial form, which comes out to be of degree 16, as anticipated in Section 2. In Section 6, we apply the presented results to a selected set of examples including broadly used commercial offset-wrist robots. Finally, Section 7 presents the conclusions and prospects for future research.

2. Distance-based problem formulation

Problems in distance geometry are formulated in terms of a set of points, P_1, \dots, P_n , and their pairwise squared distances. The squared distance between P_i and P_j is denoted as

$$s_{i,j} = s_{j,i} = \overline{P_i P_j}^2. \quad (1)$$

In our case, while some distances are constant, and can be deduced from the arm's DH parameters, others vary as the robot moves. On this basis, a lobster arm can be described as the bar-and-joint framework depicted in Fig. 2(c). Points P_2, \dots, P_6 correspond to the intersections between the six rotation axes. We assume, for the moment, that these six points are all different and proper (they are not located at infinity). P_1 and P_7 can arbitrarily be taken on the first and the last rotation axes provided that they do not coincide with P_2 and P_6 , respectively.

The origin of the reference frames for the arm's base and end-effector can be placed at P_1 and P_7 , respectively. Then, we can compute the square distances

$$s_{i,i+1} = d_i^2, \quad i = 1, \dots, 6, \quad (2)$$

where d_i is the DH parameter that accounts for the translation along the i -th z -axis. These distances are associated with the bars in blue in Fig. 2(c). Moreover, since the angle between

consecutive joint axes is known and constant (the DH parameter α_i), we can also compute, using the cosine rule for supplementary angles, the distances

$$s_{i,i+2} = d_i^2 + d_{i+1}^2 + 2d_i d_{i+1} \cos \alpha_i, \quad i = 1, \dots, 5. \quad (3)$$

These distances are associated with the bars in red in Fig. 2(c).

From the base to end-effector transform, say \mathbf{H} , we have that the homogeneous coordinates of P_6 and P_7 in the base reference frame are

$$\begin{aligned} \mathbf{p}_6 &= \mathbf{H} \mathbf{R}_x(-\alpha_6) \mathbf{T}_z(-d_6) (0, 0, 0, 1)^\top, \\ \mathbf{p}_7 &= \mathbf{H} (0, 0, 0, 1)^\top, \end{aligned}$$

where \mathbf{R}_x represents a rotation about the x -axis and \mathbf{T}_z a translation along the z -axis. Since the homogeneous coordinates of P_1 and P_2 in the base reference frame are, respectively, $\mathbf{p}_1 = (0, 0, 0, 1)$ and $\mathbf{p}_2 = (0, 0, d_1, 1)$, given \mathbf{H} we can readily determine $s_{1,6}$, $s_{1,7}$, $s_{2,6}$, and $s_{2,7}$. The corresponding bars appear in green in Fig. 2(c). Observe that these lengths do not determine the orientation of the tetrahedron $\{P_1, P_2, P_6, P_7\}$ (a tetrahedron and its mirror reflection have the same edge lengths). When several tetrahedra define the problem, it is fundamental to keep track of their relative orientations [27, 28]. Otherwise, we would generate configurations that satisfy all distance constraints but with incorrect orientations for the involved tetrahedra. Nevertheless, in this particular problem, the set of points $\{P_1, P_2, P_6, P_7\}$ defines the only tetrahedron in this problem and, as a consequence, its orientation becomes irrelevant in the formulation.

Observe that solving the inverse kinematics of the lobster arm in Fig. 2(a) is equivalent to find the assembly modes of the bar-and-joint framework in Fig. 2(c) which, in turn, is equivalent to solve the forward kinematics of the 3-4 parallel Gough-Stewart platform in Fig. 2(d). If, in this latter parallel platform, P_1 and P_7 are made to be coincident, the result is the octahedral parallel manipulator which is known to have up to 16 forward kinematic solutions [29, 30], although examples with 16 solutions are not available in the literature, up to our knowledge. Then, we have a lower bound for the number of the inverse kinematic solutions of a lobster arm, which coincides with the upper bound given by the maximum number of inverse kinematic solutions of the general 6R arm: sixteen. In other words, a lobster arm can have up to sixteen inverse kinematic solutions. An example where this occurs is given in Section 6.1.

The unknown distances in Fig. 2(c) are $s_{1,4}$, $s_{1,5}$, $s_{2,5}$, $s_{3,6}$, $s_{3,7}$, and $s_{4,7}$. It is not necessary to compute them all to obtain all possible assembly modes of this bar-and-joint framework. The problem can be reduced to compute the sets of valid values for a reduced set of unknown distances from which, together with the already known distances, the problem of giving coordinates to the seven points can be trivially solved by a series of trilaterations (or, in general, by multilaterations [31]). The number of unknown distances necessary to compute the remaining distances by trilaterations is called *coupling number*. There are problems whose coupling number is zero. This means that they can be directly solved by trilaterations. This is the case, for example, of the inverse kinematics of most wrist-partitioned 6R industrial robots [32]. Other important problems arising in robotics, such as the forward kinematics of the octahedral parallel robot [33] or the inverse kinematics of the 3R regional robot [34] have coupling number one. As we will see later, the inverse kinematics of a lobster arm is also a problem with coupling number one. The coupling number of the inverse kinematics of the general 6R arm and of the forward kinematics of the general Gough-Stewart platform are four and three [27], respectively. The coupling number is independent of the number of kinematic loops. There are problems with coupling number one and an arbitrary large number of kinematic loops, both in two [35] and three dimensions [36].

3. Basic operations with distances

3.1. Computing unknown distances from known ones

The valid distances between a set of points depends on the dimension of the embedding space. These valid distances can be characterized using the so-called Cayley-Menger determinants [37, 38]. Using Lachlan's umbral notation [39], the Cayley-Menger bi-determinant of two sets of points, P_{i_1}, \dots, P_{i_n} and P_{j_1}, \dots, P_{j_n} , is defined as

$$\Pi \begin{pmatrix} i_1, \dots, i_n \\ j_1, \dots, j_n \end{pmatrix} \triangleq \begin{vmatrix} 0 & 1 & \dots & 1 \\ 1 & s_{i_1, j_1} & \dots & s_{i_1, j_n} \\ \vdots & \vdots & \ddots & \vdots \\ 1 & s_{i_n, j_1} & \dots & s_{i_n, j_n} \end{vmatrix}. \quad (4)$$

An alternative definition (see for instance [37]) includes a multiplying constant factor which is dropped here.

If the two sets of points in (4) coincide, the resulting determinant is said to be a Cayley-Menger determinant, which we will simply denote as $\Pi(i_1, \dots, i_n)$. It comes out that a Cayley-Menger determinant is proportional to the squared volume of the simplex spanned by the involved points. Thus, in three dimensions, any Cayley-Menger determinant involving more than four points necessarily vanishes. Therefore, given five points in three dimensions, say P_i, P_j, P_k, P_l and P_m , we have that

$$\Pi(i, j, k, l, m) = 0. \quad (5)$$

This equation permits expressing any distance between these five points as a function of all other distances. In particular, for $s_{l,m}$, we have that

$$s_{l,m} = \underbrace{-\frac{1}{\Pi(i, j, k)} \left(\Pi \begin{pmatrix} i, j, k, l \\ i, j, k, m \end{pmatrix} \Big|_{s_{l,m}=0} \pm \sqrt{\Pi(i, j, k, l) \Pi(i, j, k, m)} \right)}_{\triangleq g_{l,m}(i, j, k)}, \quad (6)$$

where the notation next to the right hand side of the bideterminant indicates that all instances of $s_{l,m} = s_{m,l}$ appearing in this bideterminant are set to 0. Due to the square root, we have two possible values for $s_{l,m}$ corresponding to the two possible locations of points P_l and P_m with respect to the plane defined by $P_i, P_j,$ and P_k (see [32, 40] for details).

In two dimensions, we have that

$$\Pi(i, j, k, l) = 0 \quad (7)$$

and (6) simplifies to

$$s_{k,l} = \underbrace{-\frac{1}{\Pi(i, j)} \left(\Pi \begin{pmatrix} i, j, k \\ i, j, l \end{pmatrix} \Big|_{s_{k,l}=0} \pm \sqrt{\Pi(i, j, k) \Pi(i, j, l)} \right)}_{\triangleq g_{k,l}(i, j)}, \quad (8)$$

which, as we will see, is useful even in 3D, when dealing with coplanar points.

3.2. Trilateration

Once the problem at hand has been solved in distance space, we have to give coordinates to all points to map the result into the 3D Euclidean world. When all pairwise distances are known, this can be accomplished through the Cholesky decomposition [41]. Since this is not our case, this operation will be performed through a sequence of trilaterations.

Let us denote by \mathbf{p}_i the coordinate vector of point P_i in an arbitrary reference frame. Then, it is proved in [38] that, provided that all pairwise distances between P_i, P_j, P_k , and P_l are known, the coordinates of P_l can be computed in terms of the other point coordinates as:

$$\mathbf{p}_l = \frac{1}{k_0} (\mathbf{p}_i + k_1(\mathbf{p}_j - \mathbf{p}_i) + k_2(\mathbf{p}_k - \mathbf{p}_i) + k_3(\mathbf{p}_j - \mathbf{p}_i) \times (\mathbf{p}_k - \mathbf{p}_i)), \quad (9)$$

where

$$k_0 = -\Pi(i, j, k), \quad k_1 = \Pi\left(\begin{smallmatrix} i, k, l \\ i, j, k \end{smallmatrix}\right), \quad k_2 = -\Pi\left(\begin{smallmatrix} i, j, l \\ i, j, k \end{smallmatrix}\right), \quad k_3 = \pm \sqrt{2\Pi(i, j, k, l)}. \quad (10)$$

The square root in k_3 generates two solutions for \mathbf{p}_l , located at opposites sides of the plane supporting the triangle P_i, P_j , and P_k , which is assumed to be non-degenerate. If we have an additional distance from P_l to any point not included in the mentioned plane, then, we can determine a single solution for \mathbf{p}_l .

The position analysis of the robots with coupling number zero, or *trilaterable robots*, (both serial and parallel) can be solved by applying this operation solely. Good examples are the 3-2-1 Stewart-Gough parallel platform [42, 43] and the serial robots analyzed in [44].

3.3. From distances to angles

Once the solution has been *coordinalized*, we need to compute the robot's revolute joint angles. This is equivalent to compute some tetrahedra's dihedral angles. A nice solution to this problem can be found in [45]. Nevertheless, observe that distance-based and angle-based formulations can be seen as dual coordinate-free formulations. Thanks to a little known theorem due to M. Fiedler [46, 47], this duality arises in the form of matrix inversion.

Let us define the inverse matrix

$$\mathbf{Q}_{ijkl} = \begin{bmatrix} 0 & 1 & 1 & 1 & 1 \\ 1 & 0 & s_{i,j} & s_{i,k} & s_{i,l} \\ 1 & s_{i,j} & 0 & s_{j,k} & s_{j,l} \\ 1 & s_{i,k} & s_{j,k} & 0 & s_{k,l} \\ 1 & s_{i,l} & s_{j,l} & s_{k,l} & 0 \end{bmatrix}^{-1} \quad (11)$$

and let Λ_{ijkl} denote the tetrahedron defined by P_i, P_j, P_k and P_l . Then, the entries of $\mathbf{Q}_{ijkl} = (q_{p,q})$, $p, q = 0, \dots, 4$ have the following geometric meaning:

- $q_{0,0} = 4r^2$, r being the radius of the circumscribed sphere to Λ_{ijkl} .
- $q_{0,q} = q_{q,0}$, $q = 1, 2, 3, 4$, where $-\frac{1}{2}q_{0,q}$ are the barycentric coordinates of the circumcenter of Λ_{ijkl} . That is, the center of this circumsphere is given by

$$\mathbf{c}_{ijkl} = -\frac{1}{2} (q_{0,1}\mathbf{p}_i + q_{0,2}\mathbf{p}_j + q_{0,3}\mathbf{p}_k + q_{0,4}\mathbf{p}_l). \quad (12)$$

- $q_{p,q}$, $p, q = 1, 2, 3, 4$, determine the dihedral interior angles of Λ_{ijkl} . Indeed, the dihedral interior angle ϕ_{ik} between the faces opposite to P_i and P_k ($i \neq k$) is given by

$$\phi_{ik} = \arccos\left(\frac{q_{ik}}{\sqrt{q_{ii}}\sqrt{q_{kk}}}\right) = \arccos\left(\frac{\Pi\left(\begin{smallmatrix} j, k, l \\ i, j, l \end{smallmatrix}\right)}{\sqrt{\Pi(j, k, l)\Pi(i, j, l)}}\right), \quad (13)$$

which can be regarded as the law of cosines generalized to a tetrahedron.

4. Deriving distance-based closure conditions for lobster arms

As already explained, once the end-effector of the analyzed lobster arm is fixed with respect to its base, the distances $s_{1,6}$, $s_{1,7}$, $s_{2,6}$, and $s_{2,7}$ become determined. Now, let us take $s_{3,6}$ as a parameter. Then, we can consecutively compute the following unknown distances as a function of $s_{3,6}$

$$s_{3,7} = g_{3,7}(1, 2, 6) = f_{1,1} + f_{2,0} X_1, \quad (14)$$

$$s_{4,7} = g_{4,7}(2, 3, 6) = (f_{3,2} + f_{4,1} X_1 + f_{5,0} X_2)/f_{6,2}, \quad (15)$$

$$s_{5,7} = g_{5,7}(3, 4, 6) = (f_{7,4} + f_{8,3} X_1 + f_{9,2} X_2 - f_{6,2} X_3)/(f_{6,2} f_{10,2}). \quad (16)$$

where

$$X_1 = \pm \sqrt{f_{11,2}}, \quad (17)$$

$$X_2 = \pm \sqrt{f_{12,2} (f_{13,2} + f_{14,1} X_1)}, \quad (18)$$

$$X_3 = \pm \sqrt{f_{15,2} (f_{16,6} + f_{17,5} X_1 + f_{18,2} f_{19,2} X_2 + f_{18,2} f_{20,1} X_1 X_2)/f_{6,2}^2}, \quad (19)$$

and where $f_{i,j}$ are polynomials of degree j in $s_{3,6}$ whose symbolic expression, in terms of all robot parameters, cannot be included here due their length. We include them for a particular case with 16 real inverse kinematic solutions in the Appendix of this paper.

Since $s_{5,7}$ is one of the initially known distances, (16) can be readily rewritten as

$$f_{21,4} + f_{8,3} X_1 + f_{9,2} X_2 - f_{6,2} X_3 = 0, \quad (20)$$

which is a distance-based closure condition in the unknown distance $s_{3,6}$ for any lobster arm with

$$f_{21,4} = f_{7,4} - s_{5,7} f_{6,2} f_{10,2}. \quad (21)$$

Since X_1 , X_2 , and X_3 are nested, if we chose one of the two possible values for X_1 , we obtain two possible values for X_2 . Likewise, given one possible value of X_1 and X_2 , we obtain two possible values for X_3 . As a consequence, the closure condition given in (20) has eight branches which should be independently explored if we attempt to numerically solve it for $s_{3,6}$. Although using a numerical approach might be of interest in very large problems, in the problem treated here it is much more reasonable to derive a closure polynomial from (20) by clearing radicals.

Note that we use the term *closure polynomial* instead of *characteristic polynomial* —as in, for example, [22]— because this polynomial cannot be interpreted without stating in which variable is expressed and, as a consequence, it is not unique. Indeed, other closure conditions can of course be obtained in other unknown distances which, for the general case, do not seem to be superior in any respect to the one just obtained. Nevertheless, it cannot be excluded that a sequence might be better than another, in terms of simplicity, depending on the problem.

5. Clearing radicals

The closure condition in (20) contains nested radicals. That is, expressions containing square roots that contain other radical expressions. Euler already attempted to simplify such kind of expressions [48, §671-681]. Unfortunately, denesting is not always possible, and, even when possible, it is often difficult [49, Chapter 4]. In our case, it would involve the computation of the Galois group of the polynomials inside the square root signs which is far from trivial [50]. Moreover, denesting does not alter, in general, the number of total square roots. As it does not seem to provide any important simplification to our problem, we will simply focus on directly clearing radicals without any kind of preprocessing.

Clearing the radicals in our closing condition (20) can be achieved by iteratively isolating one radical at a time and squaring both sides of the resulting equation till no radical remains. In our case, we have to first isolate X_3 in (20) because it contains X_2 and X_1 . After squaring both sides of the equation and reorganizing the resulting terms, we obtain:

$$h_{1,8} + h_{2,7} X_1 + h_{3,6} X_2 + h_{4,5} X_1 X_2 = 0, \quad (22)$$

where

$$\begin{aligned} h_{1,8} &= -f_{11,2} f_{8,3}^2 - f_{12,2} f_{13,2} f_{9,2}^2 + f_{15,2} f_{16,6} - f_{21,4}^2, \\ h_{2,7} &= f_{15,2} f_{17,5} - f_{12,2} f_{14,1} f_{9,2}^2 - 2 f_{21,4} f_{8,3}, \\ h_{3,6} &= f_{15,2} f_{18,2} f_{19,2} - 2 f_{21,4} f_{9,2}, \\ h_{4,5} &= f_{15,2} f_{18,2} f_{20,1} - 2 f_{8,3} f_{9,2}. \end{aligned}$$

Now, after isolating X_2 in (22), squaring again both sides of the equation, and rearranging terms, we obtain

$$k_{1,16} + k_{2,15} X_1 = 0, \quad (23)$$

where

$$\begin{aligned} k_{1,16} &= f_{11,2} f_{12,2} f_{13,2} h_{4,5}^2 + 2 f_{11,2} f_{12,2} f_{14,1} h_{3,6} h_{4,5} + f_{12,2} f_{13,2} h_{3,6}^2 - f_{11,2} h_{2,7}^2 - h_{1,8}^2, \\ k_{2,15} &= f_{11,2} f_{12,2} f_{14,1} h_{4,5}^2 + 2 f_{12,2} f_{13,2} h_{3,6} h_{4,5} + f_{12,2} f_{14,1} h_{3,6}^2 - 2 h_{1,8} h_{2,7} \end{aligned}$$

Finally, after repeating the same operation with X_1 , we obtain

$$k_{2,15}^2 f_{11,2} - k_{1,16}^2 = 0, \quad (24)$$

which is the closing condition in polynomial form. This polynomial can be factorized into one term of degree 16 and in $f_{6,2}^4$ and $f_{10,2}^4$. The two later factors are singularity terms that vanish when the triangles $\widehat{P_2 P_3 P_6}$ and $\widehat{P_3 P_4 P_6}$ degenerate [51]. Each real root of the 16th-degree polynomial term in $s_{3,6}$ will satisfy (20) for a particular combination of signs for X_1 , X_2 , and X_3 . These signs are important because they give information on the location of P_3 and P_7 with respect to the plane defined by $\{P_1, P_2, P_6\}$, P_4 and P_7 with respect to the plane defined by $\{P_2, P_3, P_6\}$, and P_5 and P_7 with respect to the plane defined by $\{P_3, P_4, P_6\}$, respectively. This allows us to compute the valid lobster arm configurations by choosing the right solution, out of the two possibilities, in the subsequent trilaterations.

6. Examples

6.1. General lobster arm with 16 real inverse kinematic solutions

Using the DH parameters and the base-hand transformation given in Fig. 3(a) and (b), respectively, the procedure presented in the previous section leads to the following closure polynomial in $s_{3,6}$:

$$\begin{aligned} & s_{3,6}^{16} - 26.6700s_{3,6}^{15} + 324.733s_{3,6}^{14} - 2391.80s_{3,6}^{13} + 11905.7s_{3,6}^{12} - 42391.6s_{3,6}^{11} \\ & + 111496.0s_{3,6}^{10} - 220630.0s_{3,6}^9 + 331546.0s_{3,6}^8 - 379279.0s_{3,6}^7 + 329062.0s_{3,6}^6 \\ & - 214256.0s_{3,6}^5 + 102690.0s_{3,6}^4 - 35058.1s_{3,6}^3 + 8050.91s_{3,6}^2 - 1112.91s_{3,6} + 69.8871. \end{aligned} \quad (25)$$

This polynomial has the 16 real roots shown in Fig. 3(c). For each of these roots, we can determine the signs of X_1 , X_2 and X_3 that satisfy (20). Then, given these signs, we can compute $s_{3,7}$ and $s_{4,7}$ using (15) and (16), respectively. The corresponding signs and values of $s_{4,7}$ and (15) are also shown in Fig. 3(c). Given $s_{3,6}$, $s_{3,7}$ and $s_{4,7}$, and taking into account that P_1 , P_2 , P_6 , and P_7 are already fixed, we can compute the location of points P_3 , P_4 , and P_5 applying the following sequence of trilaterations using Eq. (9): \mathbf{p}_3 from \mathbf{p}_1 , \mathbf{p}_2 , and \mathbf{p}_6 , \mathbf{p}_4 from \mathbf{p}_2 , \mathbf{p}_3 , and \mathbf{p}_6 , and \mathbf{p}_5 from \mathbf{p}_3 , \mathbf{p}_4 , and \mathbf{p}_6 . From these points, we can obtain the robot configuration following the procedure described in Section 3.3. The robot poses obtained using this procedure are depicted in Fig. 4.

Obtaining this example with 16 real inverse kinematic solutions was not a trivial task. The discovery of a similar example for the general 6R arm by R. Manseur and K. Doty in 1989 was considered, at that time, as highly relevant, despite it was obtained rather by chance using a random search [52]. In our case, a random search led us to a maximum of 14 real solutions [53]. Fortunately, using the equivalence of lobster arms and 4-3 Stewart-Gough platforms in terms of distances, we could apply Dietmayer's method [54] to maximize the number of real solutions thus obtaining the example given above.

6.2. A wrist-partitioned lobster arm

The vast majority of commercial 6R robots are wrist-partitioned robots. They have the important advantage that analytic closed-form solution exist for their inverse kinematics [21].

To find a distance-based model of a wrist-partitioned lobster arm, we have to reorganized the seven points in the bar-and-joint framework shown in Fig. 2(c) as in Fig. 5. Then, the first three axes determine the location of the wrist center (P_6), and the last three, the orientation of the robot's end-effector (hence the adjective "wrist-partitioned").

When the end-effector is fixed with respect to the base, the locations of P_1 , P_2 , P_6 , and P_7 are known. The location of P_3 can be obtained by trilateration from its distances to P_1 , P_2 , and P_6 . This operation actually leads to two possible locations for P_3 . Then, we can locate P_4 from its distances to P_2 , P_3 , and P_6 . Since we have two possible locations for P_3 , we obtain four possible locations for P_4 . Finally, the location of P_5 can be obtained from its distances to P_4 , P_6 and P_7 . Since we have four possible locations for P_4 , we obtain eight possible locations for P_5 . In sum, a decoupled lobster arm can have up to eight inverse kinematic solutions. In this case, the inverse kinematic problem has been solved without computing any closure condition. Therefore, this is a trilaterable robot. [44].

As an example, using the DH parameters and the base-hand transformation given in Fig. 6(a) and (b), respectively, we obtain the eight inverse kinematic solutions given in Fig. 6(c) whose graphical representations are depicted in Fig. 7.

This example and the one presented in the previous subsection represent the two extreme cases, in terms of complexity, that we have to face when solving the inverse kinematics of a lobster arm. Next, we focus our attention to two intermediate cases: lobster arms with two or three consecutive parallel joint axes. Both cases are of particular relevance since many commercial offset-wrist robots can be classified within one of these two categories.

6.3. Lobster arm with two consecutive parallel joint axes

Cobots, or robots intended for direct human-robot interaction within a shared space, tend to use serial kinematic architectures that are simple and inexpensive to realize compared to those using wrist-partitioned architectures. The price to pay is that their inverse kinematics are, in general, more challenging. This is the case, for example, of the FANUC CRX-10iA/L, the Cobotta CVR038, and the Kinova Gen3 Lite, to name three representative examples. These three robots have the same arrangement of joint axes, as concluded from their DH parameters (Fig. 8).

The inverse kinematics of the offset-wrist FANUC P-200e robot was reduced to finding the roots of four separate univariate polynomials in [55]. The interesting thing about this particular robot is all other robots considered in this section can be seen as a particular cases of it by simply setting its DH parameter a_4 to zero. Therefore, the approach presented in [55] could also be applied to solve the inverse kinematics of the robots in Fig. 8. Nevertheless, other ad hoc methods have been presented since then. For example, in [56], a solution via numerical optimization of a problem formulated by means of polynomials is proposed for the Kinova Gen-3 Lite. In [57], a 16-degree closure polynomial is derived for the FANUC CRX-10iA/L by first obtaining a system of closure scalar equations and then applying variable eliminations. More recently, in [58], the inverse kinematics of this latter robot is solved by using the general algorithm presented in [18] which also allows to obtain a 16-degree polynomial. Due to the complexity of the used method, this polynomial could not be obtained in generic form, it had to be obtained for each particular base-hand transformation. Moreover, this approach failed to provide the right solution when it involves joint angles equal to π due to the used half-angle tangent variable substitution.

Observe that robots in this family are lobster arms except for the two parallel consecutive joint axes. Nevertheless, since parallel joint axes can be seen as intersecting at infinity, this kind of robots can be treated as a limit case of a lobster arm. Indeed, we could obtain a closure polynomial in $s_{3,6}$ for this kind of robots by locating the intersection point between the two parallel axes at a finite point and then taking this point to infinity. Following this approach, the coefficients of the polynomial would depend on a parameter, say d . If we make $d \rightarrow \infty$, only the leading coefficient of the closure polynomial, as a polynomial in d , would be relevant. This coefficient would be the sought closure polynomial in $s_{3,6}$. We implemented this idea and it certainly works, but here we present a less computationally demanding approach that consists in substituting parallelism constraints with coplanarity constraints. The interested reader can find both implementations in the complementary multimedia material.

Let us take the FANUC CRX-10iA/L as a representative example of this family of robots. In Fig. 9(a), we have a schematic representation of the known pairwise distances between the points defining the joint axes of this robot. We have to pay attention to the role of P'_3 and P''_3 . Their locations can be obtained by trilaterations from the locations of P_1, P_2, P_4 and P_5 , but the distance constraints of P'_3 and P''_3 with respect to these other points impose that P_1, P_2, P_4 and P_5 must be coplanar. Thus, we can focus our analysis in the position analysis of the bar-and-joint framework shown in Fig. 9(b) with the extra constraint that P_1, P_2, P_4 and P_5 must be coplanar.

After taking $s_{2,5}$ as a parameter, we can apply the following resolution sequence:

$$s_{1,5} = g_{1,5}(2, 6, 7), \quad (26)$$

$$s_{1,4} = g_{1,4}(2, 5), \quad (27)$$

$$s_{2,6} = g_{2,6}(2, 4, 5). \quad (28)$$

Observe that, due to the coplanarity constraint, the second operation involves only four points.

After clearing radicals, we obtain a 16th-degree closure polynomial that factorizes in two identical 8th-degree polynomials. It is important to highlight that, in all the examples presented in this paper, the closure polynomials are obtained in generic form (that is, for arbitrary base-hand transformations) which are then particularized for the base-hand transformation used in each example. As a consequence, this factorization is an intrinsic characteristic of the analyzed robot, not of the introduced base-hand transformation. For the particular base-hand transformation in Fig. 9(c), the 8th-degree polynomial is:

$$\begin{aligned} P^8(s_{2,5}) = & s_{2,5}^8 - 1.4289s_{2,5}^7 + 0.8718199738s_{2,5}^6 - 0.2972547285s_{2,5}^5 \\ & + 0.06209835834s_{2,5}^4 - 0.008158103810s_{2,5}^3 + 0.0006595480487s_{2,5}^2 \\ & - 0.00003005347782s_{2,5} + 5.918241430 \cdot 10^{-7}. \end{aligned} \quad (29)$$

The derivation of a polynomial of degree eight instead of sixteen, as in [58], represents an important simplification. Since closure polynomials are assumed to be of the minimum possible degree, one could incorrectly infer that there is something wrong in one of the two approaches, but this is not the case. The reason behind this apparent contradiction is that the degree of the closure polynomial obtained using a distance-based formulation is equal *or lower* than the maximum number of inverse kinematic solutions. Indeed, once the solutions in distance space are obtained, they have to be mapped onto the robot's workspace (see Section 3.2), and this mapping could be one-to-many. The analysis of the FANUC CRX-10iA/L robot is an excellent example for illustrating this important fact.

The polynomial $P^8(s_{2,5})$ in (29) has eight real solutions. Nevertheless, in this particular case, they can be grouped in three sets so that the roots in each set differ in less than 10^{-9} . Thus, we can say that, up to numerical errors, this polynomial has three solutions that we denote as $s_{2,5}^a$, $s_{2,5}^b$ and $s_{2,5}^c$. The first one, $s_{2,5}^a = 0.1207$, is a double root, the second one, $s_{2,5}^b = 0.144725$ is a quadruple root and, finally $s_{2,5}^c = 0.3043$ is also a double root (Fig. 11). These solutions can be used to obtain the locations of all points from those of P_1 , P_2 , P_6 , and P_7 by applying the following sequence of n-laterations: \mathbf{p}_5 from \mathbf{p}_2 , \mathbf{p}_6 , and \mathbf{p}_7 (two solutions); \mathbf{p}_4 from \mathbf{p}_2 , \mathbf{p}_6 , with the extra constraint that it must lie on the plane defined by \mathbf{p}_2 , \mathbf{p}_6 and \mathbf{p}_7 (two solutions); \mathbf{p}_3' from \mathbf{p}_2 , \mathbf{p}_4 , and \mathbf{p}_5 (two solutions); and \mathbf{p}_3'' from \mathbf{p}_1 , \mathbf{p}_2 , \mathbf{p}_4 , and \mathbf{p}_3' (one solution).

It is interesting to observe how the three solutions of $P^8(s_{2,5})$ are mapped onto the robot's workspace. While $s_{2,5}^a$ and $s_{2,5}^c$ lead to four valid poses each, $s_{2,5}^b$ leads to eight. That is, 16 poses in total that coincide with those given in [58].

6.4. Lobster arm with three consecutive parallel joint axes

Following the criterion introduced in the previous example, the UR-3/UR-5/UR-10 family of robots, 6R cobots created by Universal Robots, and other robots with the same architecture produced by companies such as Smokie Robotics, Techman Robot, AUBO Robotics, Omron, and Doosan Robotics can be classified as lobster arms with three consecutive parallel joint axes

(Fig. 13). The analytic solution to the inverse kinematics of this kind of robots is available from multiple sources, in the form of both reports [59, 60, 61] and journal papers [62, 63, 64, 65, 66]. While most of them are based on elementary geometric approaches, some use rather sophisticated mathematical methods. For example, Zhao *et al.* solved the problem by adopting “analytical, geometric, and algebraic methods combined with the Paden–Kahan subproblem as well as matrix theory (sic)” [64]. Villalobos *et al.* devoted a series of papers to this particular kind of robots [67, 68, 69]. They obtained a system of equations from the vector loop equation using the conventional DH parameters, while paying particular emphasis to the singularity analysis. An alternative analysis with the same goals was contemporaneously presented in [70].

Here, we concentrate in the resolution of the inverse kinematics of the UR10e robot as a representative example of this family of robots. As in the previous example, we could formulate the problem as a limit case of the general lobster arm, but, again, a simpler procedure can be devised by leveraging coplanarity constraints.

The set of points defining the location of the six revolute axes of the UR10e robot (Fig. 14(a)) can be reduced to the bar-and-joint framework in Fig. 14(b). In this case, we have to introduce P'_6 to replace P_6 . This permits substituting the parallelism of $\overline{P_2P'_2}$, $\overline{P_3P'_3}$ and $\overline{P_4P_5}$ with the coplanarity of P_2 , P_3 , P_4 , and P'_6 .

As in the previous examples, the squared distances $s_{1,6}$, $s_{2,6}$, $s_{1,7}$, and $s_{2,7}$ are obtained from the base-hand transformation. Nevertheless, due to the substitution of P_6 with P'_6 , we also need to obtain the following square distances:

$$s_{1,6'} = s_{1,6} - d_4^2, \quad (30)$$

$$s_{2,6'} = s_{2,6} - d_4^2, \quad (31)$$

$$s_{6',7} = g_{6',7}(1, 2, 6), \quad (32)$$

$$s_{4,7} = g_{4,7}(5, 6, 6'). \quad (33)$$

Observe that the square root in $g_{4,7}(5, 6, 6')$ vanishes because P_5 , P_6 , and P'_6 are coplanar and, thus, we have a single solution for $s_{4,7}$.

Now, after taking $s_{2,4}$ as a parameter, the resolution sequence is simply reduced to:

$$s_{1,4} = g_{1,4}(2, 6'), \quad (34)$$

$$s_{4,7} = g_{4,7}(1, 2, 6'), \quad (35)$$

where the first operation involves only four points due to the coplanarity constraint.

A closure condition is obtained by identifying (33) and (35). That is,

$$g_{4,7}(5, 6, 6') = g_{4,7}(1, 2, 6'). \quad (36)$$

Then, using the base-hand transformation given in Fig. 15(a), and clearing the radicals in (36), one finally obtains the closure polynomial equation in $s_{2,4}$

$$s_{2,4}^4 - 4.7510s_{2,4}^3 + 8.4610s_{2,4}^2 - 6.6943s_{2,4} + 1.9854 = 0. \quad (37)$$

This equation has four real roots (1.142459, 1.151227, 1.224254, and 1.233021). Given these values for $s_{2,4}$ the locations of all points can sequentially obtained, as in the previous examples, by n-laterations. Each valid value of $s_{2,4}$ leads to two robot poses. The resulting eight solutions, in terms of joint angles, are given in Fig. 15(b). Their graphical representation appears in Fig. 16.

6.5. The inverse kinematics of a redundant lobster arm

The KUKA LBR iiwa R800 manipulator and the Kinova Jaco-2 can be classified, according to their DH parameters, as redundant lobster arms (Fig. 17(a) and (b), respectively). Their spatial configuration is determined by the location of eight points: P_1, \dots, P_8 (Fig. 17(c)). They are said to be anthropomorphic robots because P_2, P_3 , and P_4 can be seen as the centers of the shoulder, the elbow, and the wrist, respectively.

Again, the goal is to compute the robot's joint angles for a location of its end-effector. In this case, due to the robot's redundancy, the problem is expected to be more complicated as the solution should be a self-motion manifold instead of, as in the previous examples, a set of discrete solutions. Nevertheless, it is next shown how it becomes almost trivial using the proposed distance-based formulation.

The manufacturers of this kind of robots use numerical approaches to obtain the nearest solution to a given initial configuration. This is enough when there are no obstacles in the working area. However, the additional degree of freedom makes it possible, for example, to avoid obstacles or even to perform robot motions without altering the end-effector location (and hence the name of self-motion). To accurately characterize this self-motions, we cannot rely on the iterative nature of a numerical method, a closed-form solution is needed.

In 2018, Faria *et al.* presented an analytic inverse kinematic method for 7 DoF anthropomorphic manipulators. This method included a redundancy resolution scheme to avoid singularities and joint limits [71]. To address the problem of having infinite inverse kinematic solutions, the authors introduced two additional variables in the calculation of the kinematic expressions which were essentially derived from the standard matrix loop equation in homogeneous coordinates. Two years later, Doliwa followed a similar approach based in first deriving the matrix loop equation in homogeneous transformations to obtain seven non-linear equations, four of them resulting from the rotation component, and three, from the position one [72]. These equations were then solved by simple algebraic manipulations and the self-motion manifold was also characterized from simple geometric arguments. In 2021, Da Silva *et al.* presented an approach, based on Gröbner bases, whose practical relevance is unclear as it only generates an a priori undetermined number of samples on the self-motion [73].

Using a distance-based formulation, the inverse kinematic problem of the KUKA LBR iiwa R800 manipulator reduces to solving the position analysis of the bar-and-joint framework in Fig. 18. In this case, we simply need to locate P_3 because, once the location of P_3 is known, those of P_6, P_7 and P_8 readily follow using trilaterations. Therefore, only two relevant distances are unknown: $s_{1,3}$ and $s_{3,5}$. These distances are not independent and we can express $s_{1,3}$ and $s_{3,5}$ as a function of each other. That is,

$$s_{1,3} = g_{1,3}(2, 4, 5), \quad (38)$$

$$s_{3,5} = g_{3,5}(1, 2, 4). \quad (39)$$

Alternatively, we can simply express the dependency between $s_{1,3}$ and $s_{3,5}$ in implicit form as:

$$\Pi(1, 2, 3, 4, 5) = 0. \quad (40)$$

It is not difficult to prove that this implicit form defines an ellipse in the plane $(s_{1,3}, s_{3,5})$ of the form

$$a s_{1,3}^2 + b s_{3,5}^2 + c s_{1,3} s_{3,5} + d s_{1,3} + e s_{3,5} + f = 0, \quad (41)$$

whose coefficients (a, b, c, d, e, f) can be expressed as Cayley-Menger determinants [34]:

$$\begin{aligned}
 a &= \Pi(2, 4, 5), & b &= \Pi(1, 2, 4), & c &= -2 \Pi \begin{pmatrix} 2, 4, 5 \\ 1, 2, 4 \end{pmatrix}, \\
 d &= 2 \Pi \begin{pmatrix} 1, 2, 4, 5 \\ 2, 3, 4, 5 \end{pmatrix} \Big|_{s_{1,3}, s_{3,5}=0} & e &= 2 \Pi \begin{pmatrix} 1, 2, 4, 5 \\ 1, 2, 3, 4 \end{pmatrix} \Big|_{s_{1,3}, s_{3,5}=0} & f &= -\Pi(1, 2, 3, 4, 5) \Big|_{s_{1,3}, s_{3,5}=0}
 \end{aligned} \tag{42}$$

Therefore, the possible degeneracies of the self-motion manifold can be analyzed geometrically in terms of the distances involved in the problem.

The base-hand transformation in Fig. 18(a) leads to the ellipse in Fig. 18(b). Each point of this ellipse, for instance the red dot in Fig 18(b) with coordinates $s_{13} = 0.217353$ and $s_{35} = 0.143523$, determines a location for P_3 from which we can obtain those for P_6, P_7 and P_8 . This finally leads to the eight inverse kinematic solutions compiled in Fig. 18(c). The corresponding robot poses appear in Fig. 19 which can be identified using the standard convention for antropomorphic arms. If we take the left-down-noflip configuration and P_3 is allowed to trace the whole ellipse, the robot performs the self-motion represented in Fig. 21.

7. Conclusion

Some preliminary results on the application of distance geometry for solving the inverse kinematics of a lobster arm were presented in [53]. Here, we have extended these seminal ideas to solve the inverse kinematics of any 6R and 7R with consecutive coplanar revolute axes. This allows the proposed approach to solve the inverse kinematic problem for highly popular commercial robots.

We have shown how the problem can be fully formulated and solved first in terms of distances and then mapped onto the robot's workspace. This two-stage strategy has important advantages. Firstly, it needs neither half angle tangent substitutions nor variable eliminations. Secondly, no angles are involved in the generated equations. Standard formulations lead to equations involving both rotations and translations. This means that the numerical conditioning of the problem might depend on the used units for both magnitudes. Thirdly, the obtained closure polynomials are of equal or lower degree than those using standard approaches. This is because the mapping from distances to angles is, in general, one-to-many. This phenomenon appears, for example, when solving the inverse kinematics of the FANUC CRX-10ia/L robot which represents an important advantage with respect to previous approaches.

The presented examples illustrate the possibilities of the proposed approach for solving the inverse kinematics of a wide range of commercial robots. For each of them, the corresponding closure polynomial can be obtained in symbolic form as a function of the base-hand transformation. This means that, for example, the inverse kinematics of the UR10e, the AUBO-i5, or the Doosan A0509 can be solved by obtaining the roots of a precomputed eight-degree polynomial.

Two points deserve further attention. Firstly, we have observed that some serial nR robots, which do not necessarily have consecutive coplanar joints, can be converted to lobster form by expressing some distances in terms of joint angles. This is the case of the robots with symmetric DH-parameters, as recently shown in [74], and probably also the case of the serial robots classified as palindromic in [58]. Secondly, to obtain the closure polynomial of a lobster arm, we need to introduce an unknown distance as a parameter. Nevertheless, classifying all 6R robots in terms of the number of needed parameters, as it was done for all possible Gough-Stewart platform topologies in [27], is an open problem.

Acknowledgments

We would like to express our gratitude to Dr. D. H. Salunkhe and Prof. Ph. Wenger for their comments concerning the inverse kinematics of the FANUC CRX-10ia/L robot using the algorithm presented in [18]. We would also like to gratefully acknowledge the financial support of the Spanish Government through project PID2020-117509GB-I00/AEI/10.13039/50110001103.

Appendix

The three auxiliary distances computed from $s_{3,6}$ to solve the inverse kinematics of the lobster arm in distance space are

$$\begin{aligned} s_{3,7} &= f_{1,1} + f_{2,0} X_1, \\ s_{4,7} &= (f_{3,2} + f_{4,1} X_1 + f_{5,0} X_2)/f_{6,2}, \\ s_{5,7} &= (f_{7,4} + f_{8,3} X_1 + f_{9,2} X_2 - f_{6,2} X_3)/(f_{6,2} f_{10,2}). \end{aligned}$$

where

$$\begin{aligned} X_1 &= \pm \sqrt{f_{11,2}}, \\ X_2 &= \pm \sqrt{f_{12,2} (f_{13,2} + f_{14,1} X_1)}, \\ X_3 &= \pm \sqrt{f_{15,2} (f_{16,6} + f_{17,5} X_1 + f_{18,2} f_{19,2} X_2 + f_{18,2} f_{20,1} X_1 X_2)/f_{6,2}^2}. \end{aligned}$$

With the base-hand transformation in Fig. 3(b), we have that

$$\begin{aligned} f_{1,1} &= 2.6876 s_{3,6} + 0.78459, \\ f_{2,0} &= 0.20406, \\ f_{3,2} &= 6.4614 s_{3,6}^2 - 20.298 s_{3,6} + 2.5606, \\ f_{4,1} &= -0.1878 s_{3,6} + 0.63769, \\ f_{5,0} &= -1, \\ f_{6,2} &= s_{3,6}^2 - 3.1666 s_{3,6} + 0.47208, \\ f_{7,4} &= -5.5133 s_{3,6}^4 - 50.442 s_{3,6}^3 + 244.94 s_{3,6}^2 - 134.34 s_{3,6} + 13.211, \\ f_{8,3} &= -1.2397 s_{3,6}^3 + 7.0639 s_{3,6}^2 - 12.050 s_{3,6} + 4.3831, \\ f_{9,2} &= -s_{3,6}^2 + 12.913 s_{3,6} - 6.3776, \\ f_{10,2} &= s_{3,6}^2 - 24.852 s_{3,6} + 12.029, \\ f_{11,2} &= -51.984 s_{3,6}^2 + 181.52 s_{3,6} - 75.456, \\ f_{12,2} &= s_{3,6}^2 - 3.5125 s_{3,6} + 1.5274, \\ f_{13,1} &= -1.8599 s_{3,6}^2 + 12.062 s_{3,6} - 19.466, \\ f_{14,1} &= 0.19320 s_{3,6} - 0.59445, \\ f_{15,2} &= 1.5337 s_{3,6}^2 - 9.5737 s_{3,6} + 4.3785, \\ f_{16,6} &= 16.127 s_{3,6}^6 - 236.21 s_{3,6}^5 + 1055.5 s_{3,6}^4 - 1685.8 s_{3,6}^3 + 598.51 s_{3,6}^2 + 110.86 s_{3,6} - 53.341, \\ f_{17,5} &= 16.760 s_{3,6}^5 - 123.96 s_{3,6}^4 + 300.43 s_{3,6}^3 - 268.22 s_{3,6}^2 + 93.528 s_{3,6} - 10.025, \\ f_{18,2} &= s_{3,6}^2 - 4.1065 s_{3,6} + 2.3830, \\ f_{19,2} &= 8.2705 s_{3,6}^2 - 26.345 s_{3,6} + 4.3336, \\ f_{20,1} &= s_{3,6} - 0.68708. \end{aligned}$$

The process of obtaining the closure condition from these expressions is detailed in Sections 4 and 5.

References

- [1] R. Willis, On the arrangement of the joints of crustaceous animals, Transactions of the Cambridge Philosophical Society (1841).
- [2] R. Willis, Principles of Mechanism, Longmans, Green, and Co., London, 1870.
- [3] J. Duffy, S. Derby, Displacement analysis of a spatial 7R mechanism: A generalized lobster's arm, ASME Journal of Mechanical Design 101 (2) (1979). doi:10.1115/1.3454042.
- [4] F. Freudenstein, Kinematics: past, present and future, Mechanism and Machine Theory 8 (2) (1973) 151–160. doi:10.1016/0094-114X(73)90049-9.
- [5] J. Duffy, C. Crane, A displacement analysis of the general spatial 7-link 7R mechanism, Mechanism and Machine Theory 15 (3) (1980) 153–69. doi:10.1016/0094-114X(88)90107-3.
- [6] V. Murthy, K. J. Waldron, Position kinematics of the generalized lobster arm and its series-parallel dual, ASME J. of Mechanical Design 114 (3) (1992) 406–413. doi:10.1115/1.2926566.
- [7] E. Primrose, On the input-output equation of the general 7R-mechanism, Mechanism and Machine Theory 21 (6) (1986) 509–510. doi:10.1016/0094-114X(86)90134-5.
- [8] H.-Y. Lee, Analysis of a spatial mechanism (in Chinese), Master's thesis, Beijing Institute of Posts and Telecommunications (1984).
- [9] H.-Y. Lee, C.-G. Liang, A new vector theory for the analysis of spatial mechanisms, Mechanism and Machine Theory 23 (3) (1988) 209–217. doi:10.1016/0094-114X(88)90106-1.
- [10] H.-Y. Lee, C.-G. Liang, Displacement analysis of the general spatial 7-link 7R mechanism, Mechanism and machine theory 23 (3) (1988) 219–226. doi:10.1016/0094-114X(88)90107-3.
- [11] M. Raghavan, B. Roth, Kinematic analysis of the 6R manipulator of general geometry, in: The Fifth International Symposium on Robotics Research, 1990, pp. 314–320.
- [12] M. Raghavan, B. Roth, Inverse kinematics of the general 6R manipulator and related linkages, ASME J. of Mechanical Design 114 (3) (1993) 502–508. doi:10.1115/1.2919218.
- [13] Y. Wang, L.-B. Hang, T.-L. Yang, Inverse kinematics analysis of general 6R serial robot mechanism based on Gröbner base, Frontiers of Mechanical Engineering in China 1 (1) (2006) 115–124. doi:10.1007/s11465-005-0022-7.
- [14] M. Ghazvini, Reducing the inverse kinematics of manipulators to the solution of a generalized eigenproblem, in: J. Angeles, G. Hommel, P. Kovács (Eds.), Computational Kinematics, Springer Netherlands, Dordrecht, 1993, pp. 15–26. doi:10.1007/978-94-015-8192-9_2.
- [15] Z. Fu, W. Yang, Z. Yang, Solution of inverse kinematics for 6R robot manipulators with offset wrist based on geometric algebra, Journal of Mechanisms and Robotics 5 (3) (2013) 031010. doi:10.1115/1.4024239.
- [16] C. Wampler, A. Morgan, Solving the 6R inverse position problem using a generic-case solution methodology, Mechanism and Machine Theory 26 (1991) 91–106. doi:10.1016/0094-114X(91)90024-X.
- [17] D. Manocha, J. Canny, Real time inverse kinematics for general 6R manipulators, in: Proceedings 1992 IEEE International Conference on Robotics and Automation, IEEE Comput. Soc. Press, Nice, France, 1992, pp. 383–389. doi:10.1109/ROBOT.1992.220309.
- [18] M. L. Husty, M. Pfurner, H.-P. Schröcker, A new and efficient algorithm for the inverse kinematics of a general serial 6R manipulator, Mechanism and Machine Theory 42 (1) (2007) 66–81. doi:10.1016/j.mechmachtheory.2006.02.001.
- [19] S. Liu, S. Zhu, An optimized real time algorithm for the inverse kinematics of general 6R robots, in: 2007 IEEE International Conference on Control and Automation, 2007, pp. 2080–2084. doi:10.1109/ICCA.2007.4376727.
- [20] F. Groh, K. Groh, A. Verl, On the inverse kinematics of an a priori unknown general 6R-robot, Robotica 31 (3) (2013) 455–463. doi:10.1017/S0263574712000471.
- [21] D. Pieper, The kinematics of manipulators under computer control, Phd dissertation, Stanford University (1968).
- [22] C. Mavroidis, B. Roth, Structural parameters which reduce the number of manipulator configurations, ASME Journal of Mechanical Design 116 (1) (1994) 3–10. doi:10.1115/1.2919373.
- [23] P. Dietmaier, Displacement analysis of the homogeneous, orthogonal 7-link 7R space mechanism, in: S. Stifter, J. Lenarčič (Eds.), Advances in Robot Kinematics with Emphasis on Symbolic Computation, Springer, Vienna, 1991, pp. 302–309. doi:10.1007/978-3-7091-4433-6.
- [24] R. Kumar, A. Dan, K. Rama Krishna, A note on implementation of Raghavan–Roth solution for wrist-partitioned robots, in: R. Kumar, V. S. Chauhan, M. Talha, H. Pathak (Eds.), Machines, Mechanism and Robotics, Springer, Singapore, 2022, pp. 687–696. doi:10.1007/978-981-16-0550-5_68.
- [25] F. Xiao, G. Li, D. Jiang, Y. Xie, J. Yun, Y. Liu, L. Huang, Z. Fang, An effective and unified method to derive the inverse kinematics formulas of general six-dof manipulator with simple geometry, Mechanism and Machine Theory 159 (2021) 104265. doi:10.1016/j.mechmachtheory.2021.104265.
- [26] A. Angerer, M. Hofbaur, Industrial versatility of inverse kinematics algorithms for general 6R manipulators, in:

- 2013 16th International Conference on Advanced Robotics (ICAR), 2013, pp. 1–7. doi:10.1109/ICAR.2013.6766464.
- [27] J. M. Porta, F. Thomas, Yet another approach to the Gough-Stewart platform forward kinematics, in: IEEE International Conference on Robotics and Automation (ICRA), Brisbane, QLD, 2018, pp. 974–980. doi:10.1109/ICRA.2018.8460900.
- [28] F. Thomas, A distance geometry approach to the singularity analysis of 3R robots, ASME Journal of Mechanisms and Robotics 8 (1) (2015) 011001. doi:10.1115/1.4029500.
- [29] K. Hunt, P. McAree, The octahedral manipulator: Geometry and mobility, The International Journal of Robotics Research 17 (8) (1998) 868–885. doi:10.1177/027836499801700805.
- [30] N. Rojas, J. Borràs, F. Thomas, The octahedral manipulator revisited, in: 2012 IEEE International Conference on Robotics and Automation, 2012, pp. 2293–2298. doi:10.1109/ICRA.2012.6224908.
- [31] Vikas, R. K. Sahu, A review on application of laser tracker in precision positioning metrology of particle accelerators, Precision Engineering 71 (2021) 232–249. doi:10.1016/j.precisioneng.2021.03.015.
- [32] J. Porta, L. Ros, F. Thomas, Inverse kinematics by distance matrix completion, in: Proceedings of the International Workshop on Computational Kinematics (CK2005), Cassino, Italy, 2005.
- [33] N. Rojas, J. Borràs, F. Thomas, The octahedral manipulator revisited, in: 2012 IEEE International Conference on Robotics and Automation, 2012, pp. 2293–2298. doi:10.1109/ICRA.2012.6224908.
- [34] F. Thomas, A distance geometry approach to the singularity analysis of 3R robots, Journal of Mechanisms and Robotics 8 (1) (2016) 011001. doi:10.1115/1.4029500.
- [35] N. Rojas, F. Thomas, Closed-form solution to the position analysis of Watt-Baranov trusses using the bilateration method, Journal of Mechanisms and Robotics 3 (3) (2011) 031001. doi:10.1115/1.4004031.
- [36] J. M. Porta, F. Thomas, Closed-form position analysis of variable geometry trusses, Mechanism and Machine Theory 109 (2017) 14–21. doi:10.1016/j.mechmachtheory.2016.11.004.
- [37] T. Havel, Some examples of the use of distances as coordinates for Euclidean geometry, Journal of Symbolic Computation 11 (5-6) (1991) 579–593. doi:10.1016/S0747-7171(08)80120-4.
- [38] F. Thomas, L. Ros, Revisiting trilateration for robot localization, IEEE Transactions on Robotics 21 (1) (2005) 93–101. doi:10.1109/TR0.2004.833793.
- [39] R. Lachlan, On systems of circles and spheres, Philosophical Transactions of the Royal Society of London 177 (1886) 481–625. doi:10.1098/rstl.1886.0016.
- [40] N. Rojas, F. Thomas, The closure condition of the double banana and its application to robot position analysis, in: IEEE International Conference on Robotics and Automation (ICRA), Karlsruhe, Germany, 2013, pp. 4641–4646. doi:10.1109/ICRA.2013.6631237.
- [41] M. J. Sippl, H. A. Scheraga, Solution of the embedding problem and decomposition of symmetric matrices, Proceedings of the National Academy of Sciences 82 (8) (1985) 2197–2201. doi:10.1073/pnas.82.8.2197.
- [42] H. Bruyninckx, Forward kinematics for Hunt–Primrose parallel manipulators, Mechanism and Machine Theory 34 (4) (1999) 657–664. doi:10.1016/S0094-114X(98)00010-X.
- [43] J. Andrade-Cetto, F. Thomas, A wire-based active tracker, IEEE Transactions on Robotics 24 (3) (2008) 642–651. doi:10.1109/TR0.2008.924260.
- [44] J. M. Porta, L. Ros, F. Thomas, On the trilaterable six-degree-of-freedom parallel and serial manipulators, in: IEEE International Conference on Robotics and Automation (ICRA), 2005, pp. 960–967. doi:10.1109/ROBOT.2005.1570241.
- [45] K. Wirth, A. S. Dreiding, Relations between edge lengths, dihedral and solid angles in tetrahedra, Journal of Mathematical Chemistry 52 (6) (2014) 1624–1638. doi:10.1007/s10910-014-0342-0.
- [46] M. Fiedler, Über die qualitative Lage des Mittelpunktes der umgeschriebenen Hyperkugel im n -Simplex, Commentationes Mathematicae Universitatis Carolinae 002 (1) (1961) 3–51.
URL <http://eudml.org/doc/16020>
- [47] M. Fiedler, Ultrametric sets in Euclidean point spaces, The Electronic Journal of Linear Algebra 3 (1998). doi:10.13001/1081-3810.1012.
- [48] L. Euler, Elements of Algebra, CreateSpace, Inc. & Kindle Direct Publishing, 2006.
- [49] D. J. Jeffrey, A. D. Rich, Simplifying square roots of square roots by denesting, in: M. J. Wester (Ed.), Computer Algebra Systems. A practical Guide, John Wiley & Sons, Chichester, UK, 1999, Ch. 5, pp. 61–72.
- [50] S. Landau, Simplification of nested radicals, SIAM Journal on Computing 21 (1) (1992) 85–110. doi:10.1137/0221009.
- [51] F. Thomas, J. M. Porta, Closure Polynomials for Strips of Tetrahedra, Vol. 4, Springer International Publishing, Cham, 2018, pp. 303–312. doi:10.1007/978-3-319-56802-7_32.
- [52] R. Manseur, K. L. Doty, A robot manipulator with 16 real inverse kinematic solution sets, The International Journal of Robotics Research 8 (5) (1989) 75–79. doi:10.1177/027836498900800507.
- [53] F. Thomas, J. M. Porta, The Distance Geometry of the Generalized Lobster’s Arm, Vol. 24, Springer International Publishing, Cham, 2022, p. 409–417. doi:10.1007/978-3-031-08140-8_44.

- [54] P. Dietmaier, The Stewart-Gough platform of general geometry can have 40 real postures, in: J. Lenarčič, M. L. Husty (Eds.), *Advances in Robot Kinematics: Analysis and Control*, Springer, Dordrecht, 1998, pp. 7–16. doi:10.1007/978-94-015-9064-8_1.
- [55] C. Trinh, D. Zlatanov, M. Zoppi, R. Molfino, A geometrical approach to the inverse kinematics of 6R serial robots with offset wrists, in: *Volume 5C: 39th Mechanisms and Robotics Conference*, American Society of Mechanical Engineers, Boston, Massachusetts, USA, 2015, p. V05CT08A016. doi:10.1115/DETC2015-47950.
- [56] H. M. Zohour, B. Belzile, D. St-Onge, Kinova Gen3 Lite manipulator inverse kinematics: optimal polynomial solution, arXiv:2102.01217v (2021).
- [57] L. Carbonari, M.-C. Palpacelli, M. Callegari, Inverse kinematics of a class of 6R collaborative robots with non-spherical wrist, *Robotics* 12 (2) (2023) 36. doi:10.3390/robotics12020036.
- [58] D. H. Salunkhe, *Robots cuspidaux: étude théorique, classification et applications aux robots commerciaux* (title in French, but text in English), Phd dissertation, École Centrale de Nantes (2023).
- [59] K. P. Hawkins, *Analytic inverse kinematics for the universal robots UR-5/UR-10 arms*, Tech. rep., Georgia Institute of Technology, accessed: 2010-09-30 (2013).
URL <https://repository.gatech.edu/server/api/core/bitstreams/e56759bc-92c8-43df-aa62-0dc47581459d/content>
- [60] R. Keating, N. J. Cowan, *UR5 inverse kinematics*, Tech. rep., Johns Hopkins University, accessed: 2010-09-30 (2016).
URL <https://repository.gatech.edu/server/api/core/bitstreams/e56759bc-92c8-43df-aa62-0dc47581459d/content>
- [61] R. S. Andersen, *Kinematics of a UR5*, Tech. rep., Aalborg University, accessed: 2010-09-30 (2018).
URL <https://es.scribd.com/document/442291403/ur5-kinematics>
- [62] P. M. Kebria, S. Al-wais, H. Abdi, S. Nahavandi, Kinematic and dynamic modelling of UR5 manipulator, in: 2016 IEEE International Conference on Systems, Man, and Cybernetics (SMC), IEEE, Budapest, Hungary, 2016, pp. 004229–004234. doi:10.1109/SMC.2016.7844896.
- [63] Q. Liu, D. Yang, W. Hao, Y. Wei, Research on kinematic modeling and analysis methods of UR robot, in: 2018 IEEE 4th Information Technology and Mechatronics Engineering Conference (ITOEC), IEEE, Chongqing, China, 2018, pp. 159–164. doi:10.1109/ITOEC.2018.8740681.
- [64] R. Zhao, Z. Shi, Y. Guan, Z. Shao, Q. Zhang, G. Wang, Inverse kinematic solution of 6R robot manipulators based on screw theory and the Paden–Kahan subproblem, *International Journal of Advanced Robotic Systems* 15 (6) (2018) 172988141881829. doi:10.1177/1729881418818297.
- [65] O. Abdelaziz, M. Luo, G. Jiang, S. Chen, *Multiple configurations for puncturing robot positioning*, *International Journal of Advance Robotics & Expert Systems (JARES)* 1 (4) (2019) 1–19.
URL <https://api.semanticscholar.org/CorpusID:70350054>
- [66] J. Capco, M. S. E. Din, J. Schicho, Robots, computer algebra and eight connected components, in: *Proceedings of the 45th International Symposium on Symbolic and Algebraic Computation*, ACM, Kalamata, Greece, 2020, pp. 62–69. doi:10.1145/3373207.3404048.
- [67] J. Villalobos, I. Y. Sanchez, F. Martell, Statistical comparison of Denavit-Hartenberg based inverse kinematic solutions of the UR5 robotic manipulator, in: 2021 International Conference on Electrical, Computer, Communications and Mechatronics Engineering (ICECCME), IEEE, Mauritius, 2021, pp. 1–6. doi:10.1109/ICECCME52200.2021.9591104.
- [68] J. Villalobos, I. Y. Sanchez, F. Martell, Singularity analysis and complete methods to compute the inverse kinematics for a 6-DOF UR-type robot, *Robotics* 11 (6) (2022) 137. doi:10.3390/robotics11060137.
- [69] J. Villalobos, I. Y. Sanchez, F. Martell, *Alternative Inverse Kinematic Solution of the UR5 Robotic Arm*, Vol. 347, Springer International Publishing, Cham, 2022, pp. 200–207. doi:10.1007/978-3-030-90033-5_22.
- [70] L.-T. Schreiber, C. Gosselin, Determination of the inverse kinematics branches of solution based on joint coordinates for universal robots-like serial robot architecture, *Journal of Mechanisms and Robotics* 14 (3) (2022) 034501. doi:10.1115/1.4052805.
- [71] C. Faria, F. Ferreira, W. Erlhagen, S. Monteiro, E. Bicho, Position-based kinematics for 7-dof serial manipulators with global configuration control, joint limit and singularity avoidance, *Mechanism and Machine Theory* 121 (2018) 317–334. doi:10.1016/j.mechmachtheory.2017.10.025.
- [72] S. Doliwa, Inverse kinematics of the KUKA LBR iiwa R800 (7 DOF), Tech. rep. (2020). doi:DOI10.5281/zenodo.4063574.
- [73] S. R. X. Da Silva, L. Schnitman, V. Cesca Filho, A solution of the inverse kinematics problem for a 7-degrees-of-freedom serial redundant manipulator using Gröbner bases theory, *Mathematical Problems in Engineering* 2021 (2021) 1–14. doi:10.1155/2021/6680687.
- [74] F. Thomas, B. Bongardt, *Ellipse Distance Geometry and the Design of 3R Robots*, Vol. 147, Springer Nature Switzerland, Cham, 2023, p. 577–587. doi:10.1007/978-3-031-45705-0_56.

List of Figures

1 Willis' depiction of the common crab's claw that he used to explain how its joint axes are arranged (adapted from [2, p. 462]). 22

2 (Schematic representation of a general 6R lobster arm (a) and its standard DH parameters (b) (the parameters marked with an asterisk can take any arbitrary real value as they can be incorporated into the base or the hand robot transformations). Associated bar-and-joint framework (c) (see text for the used bar color code) and kinematically equivalent 3-4 parallel Gough-Stewart platform (d). 23

3 DH parameters (a) and base-hand transformation (b) of a lobster arm with 16 real inverse kinematic solutions (c). 24

4 Representation of the 16 inverse kinematics solutions for the lobster arm with the DH parameters and hand-base transformation given in Fig. 3(a) and (b), respectively. 25

5 Bar-and-joint framework for a wrist-partitioned lobster arm. Bar color code is the same as in Fig. 2(c). 26

6 DH parameters of a decoupled lobster arm (a), used base-hand transformation (b), and the resulting eight inverse kinematics solutions (c). 27

7 The eight inverse kinematics solutions of the decoupled lobster arm given in Fig. 6. 28

8 The FANUC CRX-10iA/L (a), the Cobotta CVR038 (b), and the Kinova Gen3 Lite (c) have the same arrangement of joint axes. They are offset-wrist 6R robots which can be seen as lobster arms. 29

9 Schematic representation of the known pairwise distances between the pairs of points defining the joint axes in the FANUC CRX-10iA/L (a). Since the locations of points P'_3 and P''_3 can be obtained by trilaterations from the locations of the other points, we have to focus our analysis in the location of the points shown in the bar-and-joint framework in (b). The nodes in black correspond to points that must be coplanar. The bar color code is the same as in Fig. 2(c). 30

10 (a) Base-hand transformation for the FANUC CRX-10iA/L, and (b) the resulting inverse kinematics solutions. 31

11 Plot of function $P^8(s_{2,5})$ in (29) in linear and logarithm scale. Three roots, of multiplicity 2, 4, and 2 are located at $s_{2,5}^a$, $s_{2,5}^b$, and $s_{2,5}^c$, respectively. Due to the even multiplicity of all roots, the function is positive in all its range. 32

12 The sixteen inverse kinematics solutions of the FANUC CRX-10A/L for the base-hand transformation given in Fig. 7(a). 33

13 The UR10e (a), the AUBO-i5 (b), and the TM5-700 (c) have the same arrangement of joint axes, as it can be verified from their DH parameters. Their second, third and fourth revolute axes are parallel. 34

14 Schematic representation of the known distances between the points defining the joint axes in the UR10e robot (a). By replacing P_6 with P'_6 , the analysis can be reduced to finding the location of the points shown in the bar-and-joint framework in (b), where nodes in black correspond to points that must be coplanar. Distance h can take any non-null arbitrary value. Again, the bar color code is the same as in Fig. 2(c). 35

15 The base-hand transformation for the UR10e robot given in (a) leads to the eight inverse kinematic solutions given in (b). 36

16 Representation of the eight inverse kinematic solutions given in Fig. 15(b). 37

17	The KUKA LBR iiwa R800 manipulator (a) and the Kinova Jaco-2 (b) are redundant serial robots that can be classified as lobster arms, as it can be verified from their DH parameters. Despite their apparent complexity, their inverse kinematics can be formulated in terms of only eight points (c), where the seven rotation axes are determined by $\overline{P_1P_2}$, $\overline{P_2P_6}$, $\overline{P_2P_3}$, $\overline{P_3P_7}$, $\overline{P_3P_4}$, $\overline{P_4P_8}$ and $\overline{P_4P_7}$	38
18	Bar-and-joint framework associated with the robots in Fig. 17. In this case, we just need to locate P_3 because the locations of P_6 , P_7 and P_8 become readily determined, once that of P_3 is known, using trilaterations.	39
19	For the shown robot's end-effector location in (a), the valid values of s_{13} and s_{35} are on an ellipse (b). Each point of this ellipse defines a location for P_3 . Then, we can compute the two possible locations for P_6 , P_7 , and P_8 with respect to the triangles $\widehat{P_1P_2P_3}$, $\widehat{P_2P_3P_4}$, and $\widehat{P_3P_4P_5}$, respectively, using trilateration. Thus, each point of the ellipse determines eight inverse kinematic solutions. For example, for the point in marked in red, we obtain the eight inverse kinematic solutions shown in (c).	40
20	Representation of the eight inverse kinematic solutions in Fig. 18(c). Each of these solutions can be identified with the right-left shoulder, up-down elbow, and flip-noflip wrist convention used when working with antropomorphic arms. . . .	41
21	Self-motion for the left-down-noflip configuration with the base-hand transformation given in Fig. 18(a). As in all eight configurations, the center of the elbow (P_3) can freely rotate about the line defined by the center of the shoulder (P_2) and that of the wrist (P_4).	42

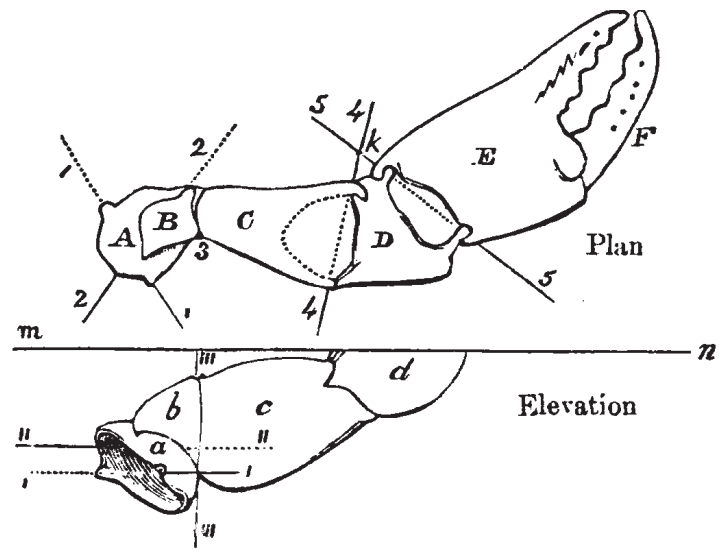


Figure 1: Willis' depiction of the common crab's claw that he used to explain how its joint axes are arranged (adapted from [2, p. 462]).

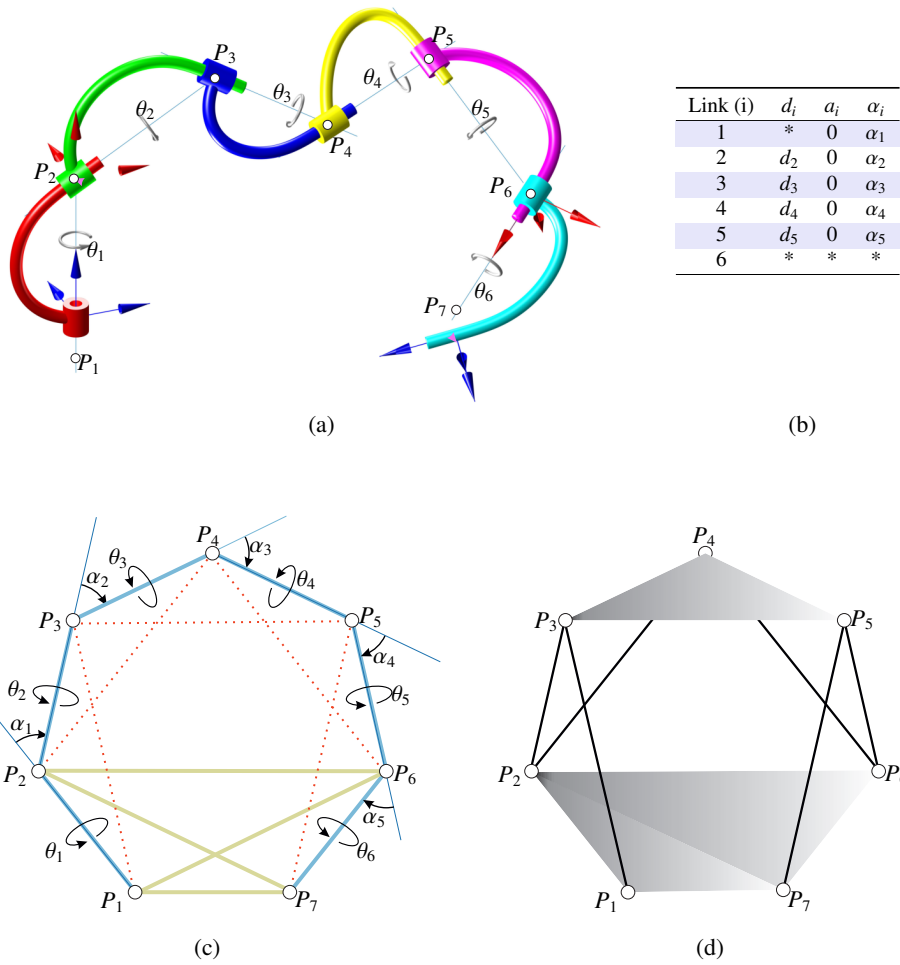


Figure 2: (Schematic representation of a general 6R lobster arm (a) and its standard DH parameters (b) (the parameters marked with an asterisk can take any arbitrary real value as they can be incorporated into the base or the hand robot transformations). Associated bar-and-joint framework (c) (see text for the used bar color code) and kinematically equivalent 3-4 parallel Gough-Stewart platform (d).

Link (i)	d_i	a_i	α_i
1	1.7516	0	1.9236
2	1.0655	0	2.3291
3	2.8190	0	2.6420
4	1.3708	0	1.0879
5	1.09690	0	1.6420
6	1.43930	0	0

(a)

$$\mathbf{H}_1 = \begin{bmatrix} 0.1911 & 0.1109 & 0.9753 & 1.9281 \\ -0.8855 & 0.4483 & 0.1225 & -0.1763 \\ -0.4236 & -0.8870 & 0.1838 & 2.2371 \\ 0 & 0 & 0 & 1.0000 \end{bmatrix}$$

(b)

sol.	$s_{3,6}$	signs	$s_{3,7}$	$s_{4,7}$	θ_1	θ_2	θ_3	θ_4	θ_5	θ_6
1	0.510315	--+	1.766871	8.368854	1.3074	-3.0444	2.1648	-0.2014	1.9112	0.0000
2	0.511531	+++	2.556932	5.349593	1.1897	-2.7579	-1.3991	0.1011	-2.2439	0.8478
3	0.517535	++-	2.611473	4.985376	-2.0683	-1.9220	-0.8527	1.5262	0.4191	1.4161
4	0.549951	-+-	1.662544	7.359441	-1.4706	0.0910	-0.5592	1.4169	1.0860	2.9248
5	0.552049	--+	1.659208	9.676559	-2.7092	3.0060	1.1400	-1.4580	-1.9520	1.1194
6	0.644244	+++	3.426636	2.921999	-1.9294	-2.8000	0.7438	-1.5152	-1.4027	1.5271
7	1.213606	+ - +	5.732403	6.754064	0.7633	2.7293	-0.6964	0.1056	-1.3257	1.5752
8	1.243517	--+	2.420891	9.612035	-1.0238	0.3476	1.5209	-1.2424	-0.9514	-2.3640
9	1.342072	+++	6.153180	3.077457	2.1407	-0.9368	-2.0707	0.7735	2.9416	-1.7570
10	2.274742	++-	8.586736	4.171884	-0.1572	-3.1410	-2.0863	0.7570	1.7317	0.0933
11	2.718666	+++	9.278002	4.570913	0.7421	2.6288	1.7610	-0.1255	1.2162	0.4594
12	2.788582	--+	7.229026	7.619825	0.4669	1.8698	-0.2408	0.3367	-0.3508	2.0134
13	2.825605	-+-	7.412886	7.492612	1.3125	-2.3084	-2.1752	0.2054	-3.0882	-0.0126
14	2.975285	+ - -	9.211062	5.612341	-0.2667	0.8603	-0.2734	0.8259	0.4635	2.6523
15	2.998423	++-	9.089404	3.050897	-2.0301	-0.8754	0.8919	-1.5241	-0.4462	-3.0215
16	3.003898	+ - +	9.033572	3.011288	-2.7632	-0.0301	-1.1731	1.4438	1.9917	-2.7305

(c)

Figure 3: DH parameters (a) and base-hand transformation (b) of a lobster arm with 16 real inverse kinematic solutions (c).

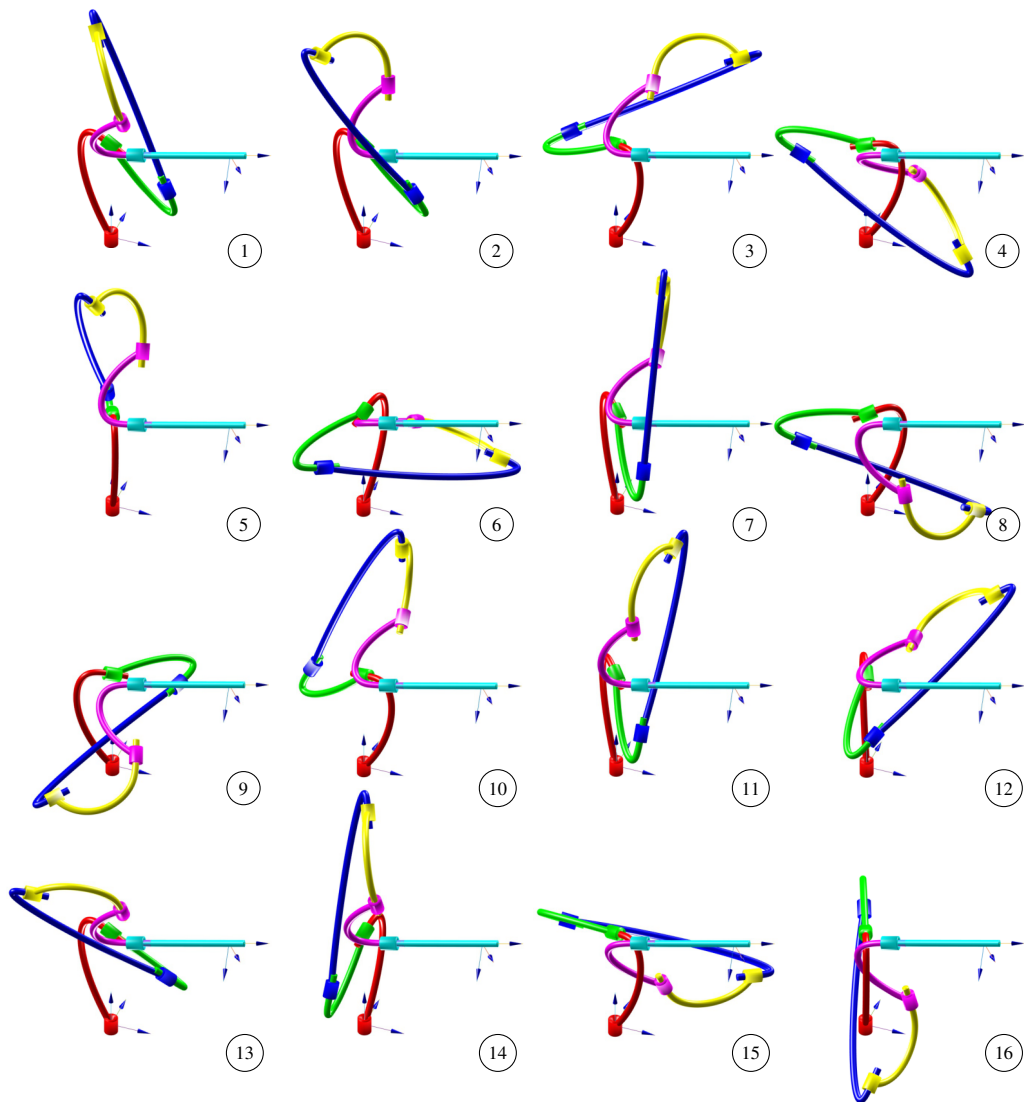


Figure 4: Representation of the 16 inverse kinematics solutions for the lobster arm with the DH parameters and hand-base transformation given in Fig. 3(a) and (b), respectively.

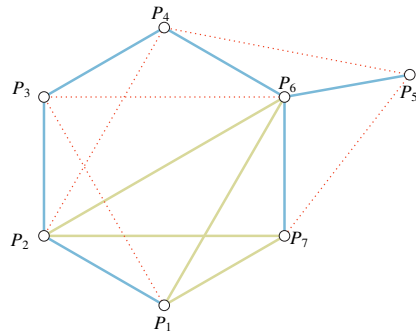


Figure 5: Bar-and-joint framework for a wrist-partitioned lobster arm. Bar color code is the same as in Fig. 2(c).

Link (i)	d_i	a_i	α_i
1	0.5	0	$\pi/2$
2	1.0	0	$\pi/2$
3	0.5	0	$\pi/2$
4	0.1	0	$\pi/2$
5	0	0	$-\pi/2$
6	0.1	0	0

(a)

$$\mathbf{H}_2 = \begin{bmatrix} 0.6849 & -0.6976 & 0.2103 & -1.0822 \\ 0.7008 & 0.7097 & 0.0720 & -0.0847 \\ -0.1995 & 0.0981 & 0.9750 & 0.6069 \\ 0 & 0 & 0 & 1 \end{bmatrix}$$

(b)

sol.	θ_1	θ_2	θ_3	θ_4	θ_5	θ_6
1	-0.6367	-1.3759	-0.6338	-1.4252	1.2710	0.8213
2	-0.6367	-1.3759	-0.6338	1.7164	-1.2710	-2.3203
3	-0.6367	-2.0587	0.6338	-1.7957	1.2162	-0.4379
4	-0.6367	-2.0587	0.6338	1.3459	-1.2162	2.7037
5	-1.8478	2.0587	-0.6338	0.9869	2.6572	-1.0252
6	-1.8478	2.0587	-0.6338	-2.1547	-2.6572	2.1164
7	-1.8478	1.3759	0.6338	2.3675	2.3413	1.3435
8	-1.8478	1.3759	0.6338	-0.7740	-2.3413	-1.7981

(c)

Figure 6: DH parameters of a decoupled lobster arm (a), used base-hand transformation (b), and the resulting eight inverse kinematics solutions (c).

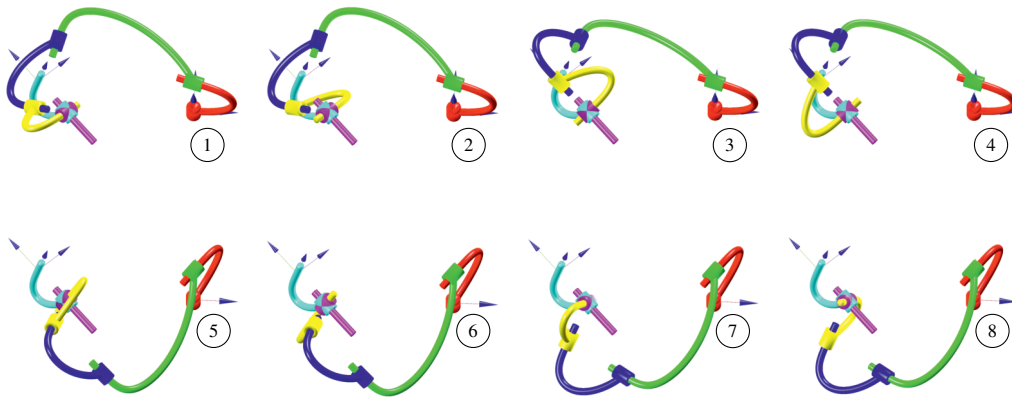


Figure 7: The eight inverse kinematics solutions of the decoupled lobster arm given in Fig. 6.



(a)

Link (i)	d_i (mm)	a_i (mm)	α_i (rad)
1	245	0	$\pi/2$
2	260	710	0
3	-260	0	$-\pi/2$
4	540	0	$\pi/2$
5	150	0	$\pi/2$
6	160	0	0



(b)

Link (i)	d_i (mm)	a_i (mm)	α_i (rad)
1	180	0	$\pi/2$
2	0	165	0
3	20.0	0	$-\pi/2$
4	177.5	0	$\pi/2$
5	38.5	0	$-\pi/2$
6	63.5	0	0



(c)

Link (i)	d_i (mm)	a_i (mm)	α_i (rad)
1	243.3	0	$\pi/2$
2	30	280	π
3	20	0	$\pi/2$
4	245	0	$\pi/2$
5	57	0	$\pi/2$
6	235	0	0

Figure 8: The FANUC CRX-10iA/L (a), the Cobotta CVR038 (b), and the Kinova Gen3 Lite (c) have the same arrangement of joint axes. They are offset-wrist 6R robots which can be seen as lobster arms.

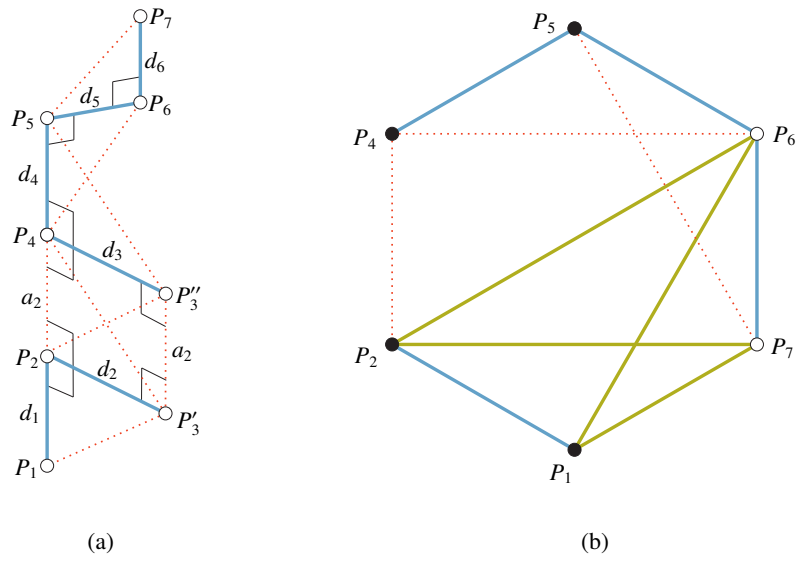


Figure 9: Schematic representation of the known pairwise distances between the pairs of points defining the joint axes in the FANUC CRX-10iA/L (a). Since the locations of points P'_3 and P''_3 can be obtained by trilaterations from the locations of the other points, we have to focus our analysis in the location of the points shown in the bar-and-joint framework in (b). The nodes in black correspond to points that must be coplanar. The bar color code is the same as in Fig. 2(c).

$$\mathbf{H}_3 = \begin{bmatrix} 1 & 0 & 0 & -0.4 \\ 0 & -1 & 0 & 0 \\ 0 & 0 & -1 & 0 \\ 0 & 0 & 0 & 1 \end{bmatrix}$$

(a)

sol.	$s_{2,5}$	signs	θ_1	θ_2	θ_3	θ_4	θ_5	θ_6
1	0.1207	- + -	-2.7688	-1.0765	1.0765	0.2400	0.0000	-2.5287
2		- + +	0.3728	-2.0651	2.0651	-2.9016	0.0000	-2.5287
3		+ - -	2.7688	-1.0765	1.0765	2.9016	-0.0000	-0.6129
4		+ - +	-0.3728	-2.0651	2.0651	-0.2400	-0.0000	-0.6129
5	0.144725	- - -	0.3844	2.5186	1.0140	-3.1416	-2.7505	-2.7572
6		- - +	-2.7572	0.6229	2.1276	-0.0000	-2.7505	-2.7572
7		- + -	-2.7572	-1.0736	1.0140	0.0000	0.0596	-2.7572
8		- + +	0.3844	-2.0680	2.1276	3.1416	0.0596	-2.7572
9		+ - -	2.7572	-1.0736	1.0140	-3.1416	-0.0596	-0.3844
10		+ - +	-0.3844	-2.0680	2.1276	-0.0000	-0.0596	-0.3844
11		+ + -	-0.3844	2.5186	1.0140	0.0000	2.7505	-0.3844
12		+ + +	2.7572	0.6229	2.1276	3.1416	2.7505	-0.3844
13	0.3043	- - -	0.0819	2.4460	0.6956	-1.7907	-3.1416	1.8726
14		- - +	-3.0597	0.6956	2.4460	1.3509	-3.1416	1.8726
15		+ + -	-0.0819	2.4460	0.6956	-1.3509	-3.1416	1.2690
16		+ + +	3.0597	0.6956	2.4460	1.7907	-3.1416	1.2690

(b)

Figure 10: (a) Base-hand transformation for the FANUC CRX-10iA/L, and (b) the resulting inverse kinematics solutions.

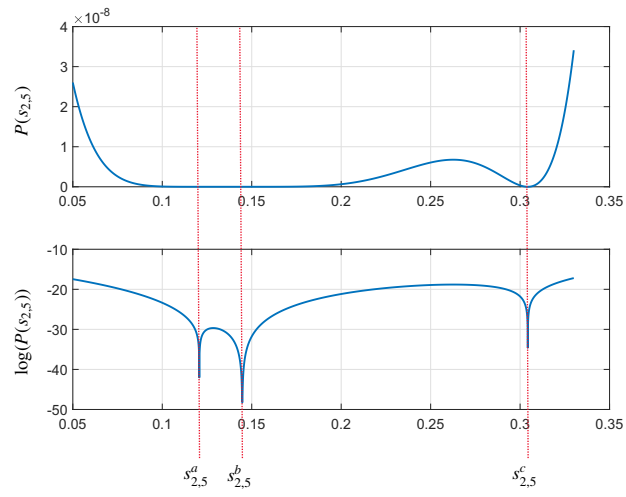


Figure 11: Plot of function $P^8(s_{2,5})$ in (29) in linear and logarithm scale. Three roots, of multiplicity 2, 4, and 2 are located at $s_{2,5}^a$, $s_{2,5}^b$, and $s_{2,5}^c$, respectively. Due to the even multiplicity of all roots, the function is positive in all its range.

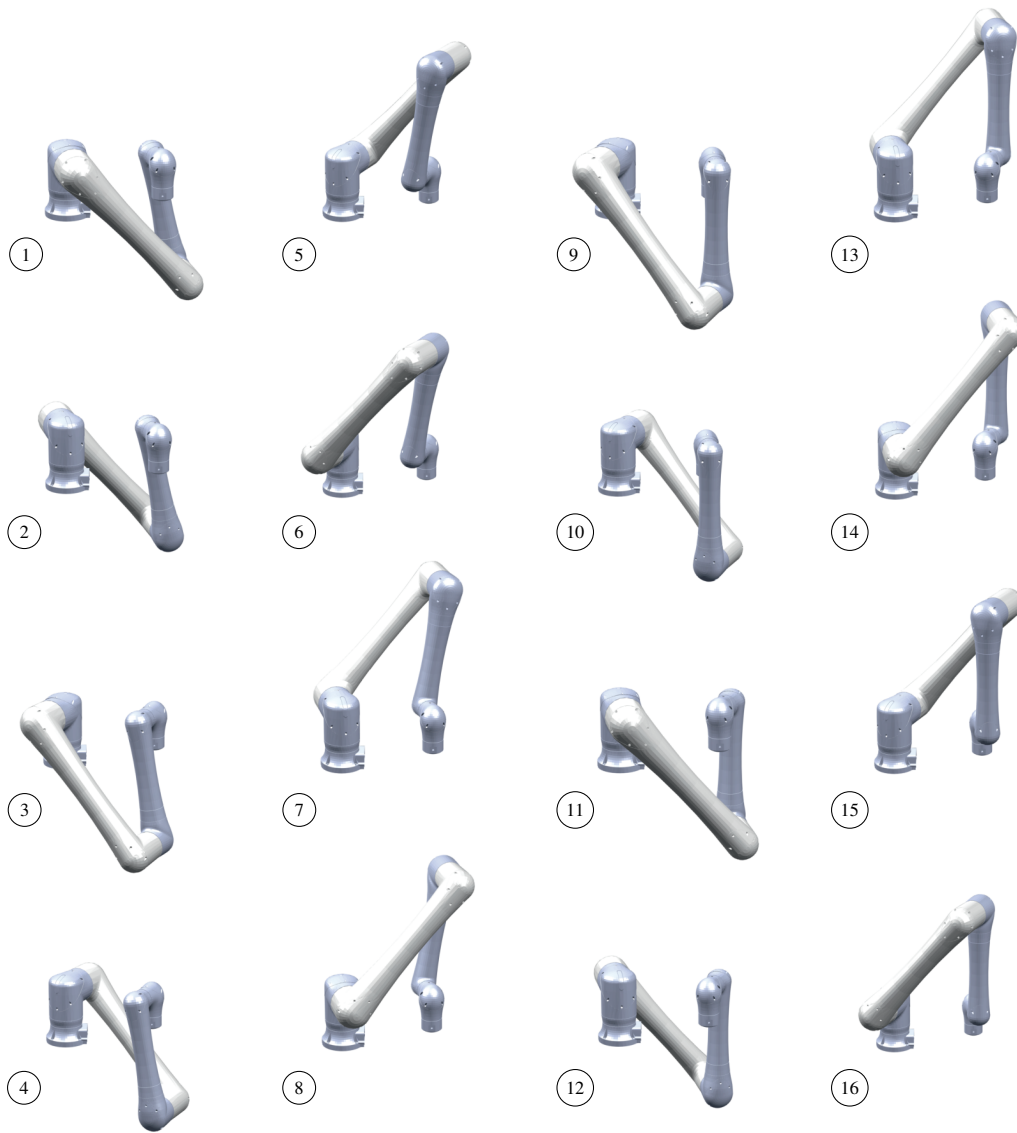


Figure 12: The sixteen inverse kinematics solutions of the FANUC CRX-10A/L for the base-hand transformation given in Fig. 7(a).



(a)

Link (i)	d_i (mm)	a_i (mm)	α_i (rad)
1	180.7	0	$\pi/2$
2	0	-612.70	0
3	0	-571.55	0
4	174.15	0	$\pi/2$
5	115.985	0	$-\pi/2$
6	116.55	0	0



(b)

Link (i)	d_i (mm)	a_i (mm)	α_i (rad)
1	96.43	0	$\pi/2$
2	0	410	0
3	100	380	0
4	20	0	$\pi/2$
5	100	0	$\pi/2$
6	80	0	0



(c)

Link (i)	d_i (mm)	a_i (mm)	α_i (rad)
1	145.1	0	$-\pi/2$
2	0	329	0
3	0	311.5	0
4	-122.2	0	$\pi/2$
5	106.0	0	$\pi/2$
6	114.4	0	0

Figure 13: The UR10e (a), the AUBO-i5 (b), and the TM5-700 (c) have the same arrangement of joint axes, as it can be verified from their DH parameters. Their second, third and fourth revolute axes are parallel.

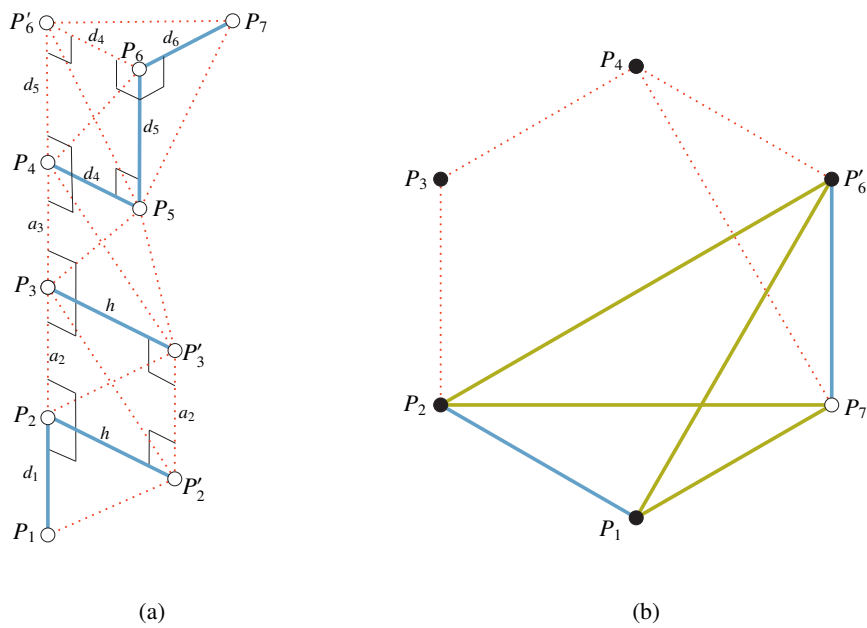


Figure 14: Schematic representation of the known distances between the points defining the joint axes in the UR10e robot (a). By replacing P_6 with P'_6 , the analysis can be reduced to finding the location of the points shown in the bar-and-joint framework in (b), where nodes in black correspond to points that must be coplanar. Distance h can take any non-null arbitrary value. Again, the bar color code is the same as in Fig. 2(c).

$$\mathbf{H}_4 = \begin{bmatrix} -0.4850 & -0.6042 & 0.6323 & 0.8797 \\ 0.7822 & -0.6230 & 0.0047 & 0.1412 \\ 0.3911 & 0.4968 & 0.7747 & 1.0026 \\ 0 & 0 & 0 & 1.0000 \end{bmatrix}$$

(a)

sol.	θ_1	θ_2	θ_3	θ_4	θ_5	θ_6
1	0.3873	-2.7223	0.8908	2.7538	-1.3341	0.3668
2	0.3873	-1.8647	-0.8908	-2.6054	-1.3341	0.3668
3	3.0999	-1.2693	0.8746	-0.4922	1.5398	0.7049
4	3.0999	-0.4272	-0.8746	0.4149	1.5398	0.7049
5	3.0999	-0.9887	0.7294	2.5140	-1.5398	-2.4367
6	3.0999	-0.2858	-0.7294	-3.0133	-1.5398	-2.4367
7	0.3873	-2.8457	0.7104	-0.0840	1.3341	-2.7747
8	0.3873	-2.1611	-0.7104	0.6521	1.3341	-2.7747

(b)

Figure 15: The base-hand transformation for the UR10e robot given in (a) leads to the eight inverse kinematic solutions given in (b).

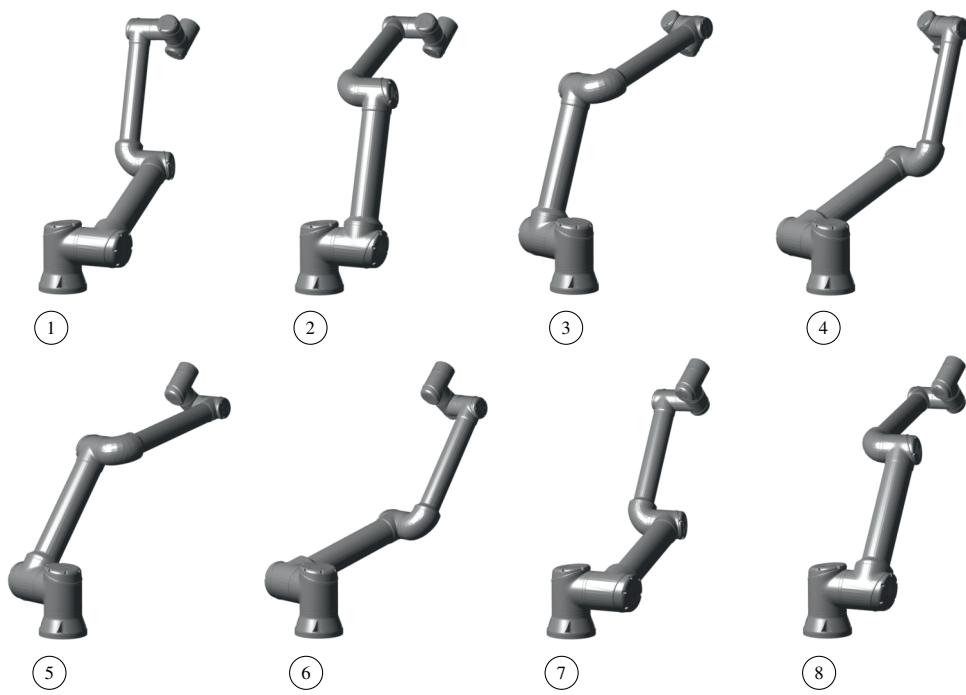
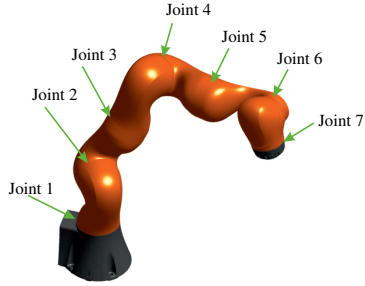
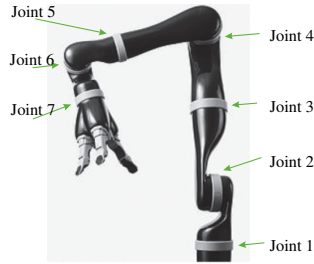


Figure 16: Representation of the eight inverse kinematic solutions given in Fig. 15(b).



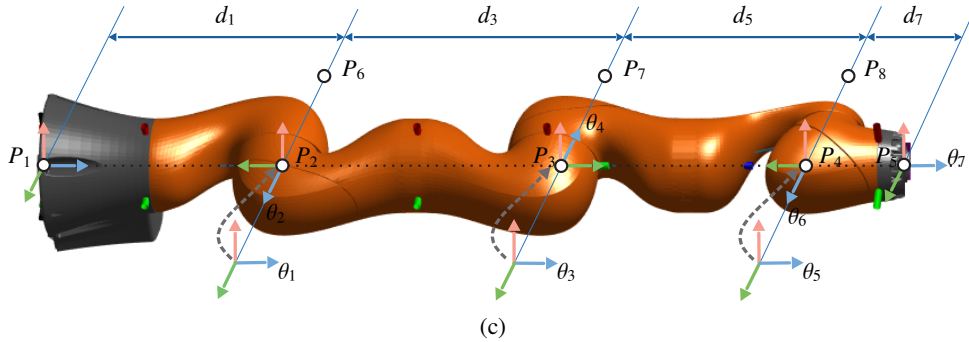
Link (i)	d_i (mm)	a_i (mm)	α_i (rad)
1	340	0	$-\pi/2$
2	0	0	$\pi/2$
3	400	0	$\pi/2$
4	0	0	$-\pi/2$
5	400	0	$-\pi/2$
6	0	0	$\pi/2$
7	126	0	0

(a)



Link (i)	d_i (mm)	a_i (mm)	α_i (rad)
1	275.5	0	$\pi/2$
2	0	0	$\pi/2$
3	410	0	$\pi/2$
4	9.8	0	$\pi/2$
5	311.1	0	$\pi/2$
6	0	0	$\pi/2$
7	263.8	0	π

(b)



(c)

Figure 17: The KUKA LBR iiwa R800 manipulator (a) and the Kinova Jaco-2 (b) are redundant serial robots that can be classified as lobster arms, as it can be verified from their DH parameters. Despite their apparent complexity, their inverse kinematics can be formulated in terms of only eight points (c), where the seven rotation axes are determined by $\overline{P_1P_2}$, $\overline{P_2P_6}$, $\overline{P_2P_3}$, $\overline{P_3P_7}$, $\overline{P_3P_4}$, $\overline{P_4P_8}$ and $\overline{P_4P_7}$.

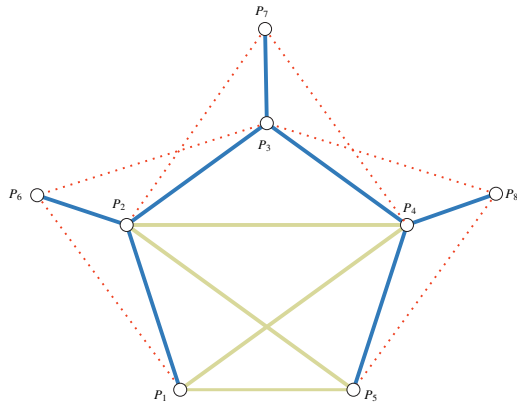
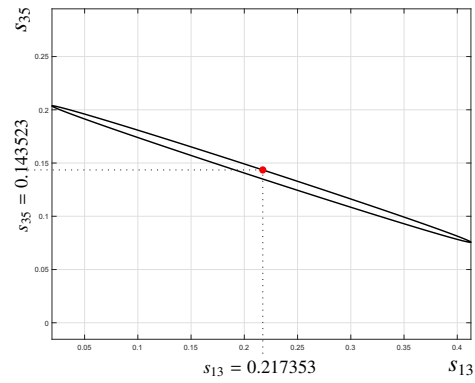


Figure 18: Bar-and-joint framework associated with the robots in Fig. 17. In this case, we just need to locate P_3 because the locations of P_6 , P_7 and P_8 become readily determined, once that of P_3 is known, using trilaterations.

$$\mathbf{H}_3 = \begin{bmatrix} -0.7945 & 0.0157 & -0.6070 & -0.3279 \\ -0.5875 & -0.2723 & 0.7620 & -0.0919 \\ -0.1533 & 0.9621 & 0.2256 & 1.0089 \end{bmatrix}$$



(a)

(b)

sol.	θ_1	θ_2	θ_3	θ_4	θ_5	θ_6	θ_7
1	1.6378	1.7866	-1.8485	1.7574	-2.0846	1.8975	1.5478
2	1.6378	1.7866	-1.8485	1.7574	1.0570	-1.8975	-1.5938
3	1.6378	1.7866	1.2931	-1.7574	1.0570	1.8975	1.5478
4	1.6378	1.7866	1.2931	-1.7574	-2.0846	-1.8975	-1.5938
5	-1.5038	-1.7866	1.2931	1.7574	-2.0846	1.8975	1.5478
6	-1.5038	-1.7866	1.2931	1.7574	1.0570	-1.8975	-1.5938
7	-1.5038	-1.7866	-1.8485	-1.7574	1.0570	1.8975	1.5478
8	-1.5038	-1.7866	-1.8485	-1.7574	-2.0846	-1.8975	-1.5938

(c)

Figure 19: For the shown robot's end-effector location in (a), the valid values of s_{13} and s_{35} are on an ellipse (b). Each point of this ellipse defines a location for P_3 . Then, we can compute the two possible locations for P_6 , P_7 , and P_8 with respect to the triangles $\widehat{P_1P_2P_3}$, $\widehat{P_2P_3P_4}$, and $\widehat{P_3P_4P_5}$, respectively, using trilateration. Thus, each point of the ellipse determines eight inverse kinematic solutions. For example, for the point in marked in red, we obtain the eight inverse kinematic solutions shown in (c).

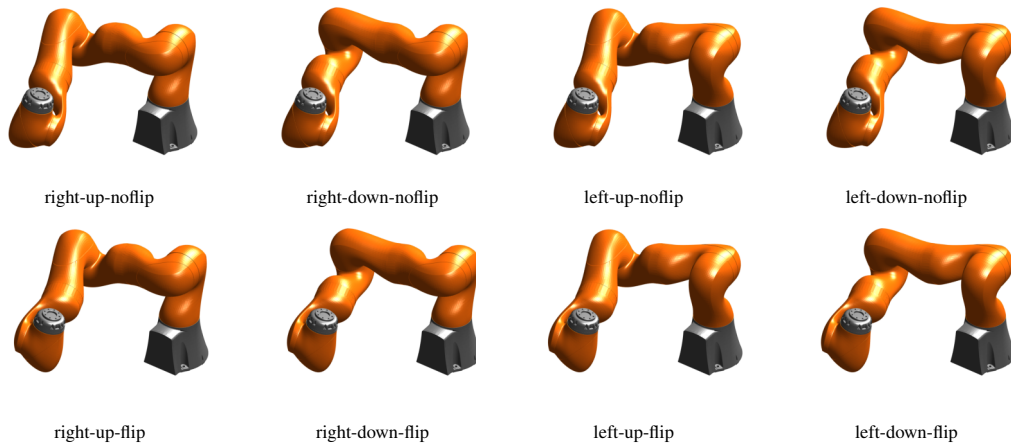


Figure 20: Representation of the eight inverse kinematic solutions in Fig. 18(c). Each of these solutions can be identified with the right-left shoulder, up-down elbow, and flip-noflip wrist convention used when working with antropomorphic arms.

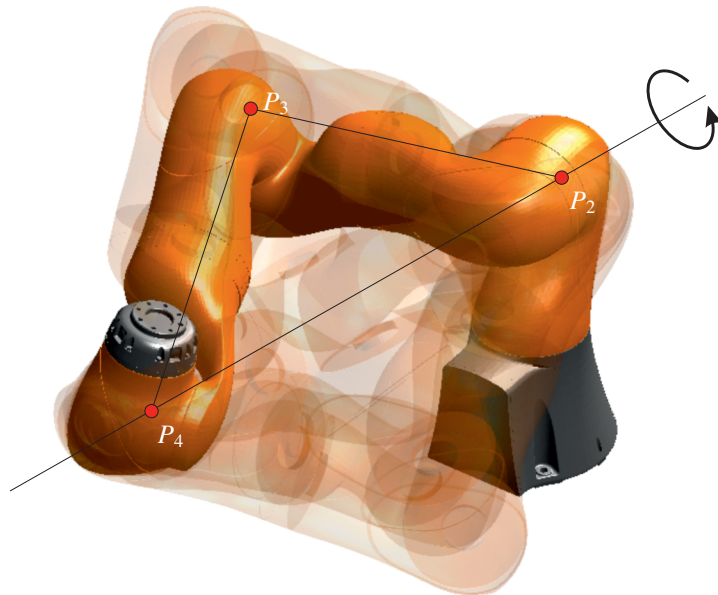


Figure 21: Self-motion for the left-down-noflip configuration with the base-hand transformation given in Fig. 18(a). As in all eight configurations, the center of the elbow (P_3) can freely rotate about the line defined by the center of the shoulder (P_2) and that of the wrist (P_4).